IOWA STATE UNIVERSITY
Digital Repository

2010

Cast data matrix symbols performance characterization

Greg Carl Saveraid
Iowa State University

Follow this and additional works at: https://lib.dr.iastate.edu/etd

Part of the Industrial Engineering Commons

Recommended Citation

www.manaraa.com

Cast data matrix symbols performance characterization

by

Greg Carl Saveraid

A thesis submitted to the graduate faculty

in partial fulfillment of the requirements of the degree of

MASTER OF SCIENCE

Major: Industrial Engineering

Program of Study Committee:
Frank E. Peters, Major Professor
Matthew Frank
Scott Chumbley

Iowa State University

Ames, Iowa

2010

Table of Contents

List of Tables

List of Figures

Acknowledgements

This document is the result of many. It would not be possible without the support of too numerous to name, but here's my best attempt. Thank you to the Steel Founders' Society for their guidance and support. Thank you to the University of Northern Iowa Metal Casting Lab for providing materials early in the experimentation process. Thank you for support from the vision system industry, including Power/mation, Cognex and specifically Echo Automation. Thank you to Wellman Dynamics Corporation, your patience as an employer is truly a testament to the care you show for your employees. Thank you for Kevin Patterson for serving as a constant sound board for experimentation ideas and strategy, your knowledge of the casting industry was invaluable and in many respects, unsurpassed. Thank you to my major professor, Dr. Frank Peters, who gave me a chance and never stopped challenging me and for that I owe a debt of gratitude. Thank you to Justin Walker, Chris Hunt, Mike Rickers, and especially Scott Von Busch for your professional and personal support; I'm still "Blinded by the Light." And most importantly thank you to my wife who provided constant encouragement needed to complete this work, I look forward to the future life ahead of us, I love you. I dedicate this to those who went before me and shaped by understanding of the world, my Grandfathers: Thomas J. Bacher and Kenneth E. Saveraid.

Abstract

Data matrix symbols are used as a robust means of unique part identification in many industries. Research of cast data matrix symbols has been limited and expected symbol performance unknown. To develop knowledge of cast data matrix symbol performance, the investigation initially focused on feasibility of casting data matrix symbol. Results of a feasibility experiment led to further investigation of cast symbol design expected performance.

Bump marks were evaluated initially due to the inherent ease of production and use in previous cast data matrix applications. The results indicate Bump mark geometry is problematic, due to the inherent nature of shadow formation as a means to create contrast marks. Using design inspiration from Dot Peen data matrix symbols, an alternative cast data matrix design was pursued and analyzed. The results of this modified Dimple mark geometry proved to be superior to the Bump contrast symbol geometry in side by side analysis. A deeper analysis at the module level was also pursued to determine the effect on Print Growth and Symbol Contrast for an array of mark diameters, spacing and surface roughness values. Also, an optimal light angle was selected based on the ANOVA analysis and Print Growth$_m$ and Symbol Contrast averages.

An applicable design was presented with the use of a heuristic to select ideal symbol factors, which indicated the physical size for aluminum cast data matrix symbols with ten and 50 character capacities were determined to be 1.75 and 3.00 inches, respectively. Using the same methodology for ferrous cast data matrix symbols with ten and 50

character capacities, the physical symbol size was determined to be 2.19 and 3.75 inches,

respectively.

1. Introduction

Unique identification of parts in a manufacturing process is a tool that provides engineers and managers with information for making informed decisions. The implementation of unique product identification in the foundry industry that is repeatable and reliable would enable increased use of lean manufacturing practices and other process improvement methods. Typical methods to identify castings include the following:

- adhesive labels
- cast serial numbers
- vibratory peening
- imbedded RFID tag

There are significant drawbacks to the use of these methods. Adhesive labels cannot withstand abrasive foundry processes such as shot blasting or heat treatment. Cast or vibratory peened serial numbers have limited data capacity and are subject to human error or data loss in the event a character is destroyed. Research into imbedded RFID tags indicated success through insulating tags and casting into parts [1]. However, this approach is unacceptable in some applications where quality requirements prevent the inclusion of tags into casting base metal due to the need to prevent stress risers in cast parts. All these methods do not utilize the basic advantage of the casting process which is the ability to create complex geometry while being both inexpensive and efficient.

Barcodes are widely used as printed symbols in various applications. Barcodes can also be impressed or etched onto metal or solid substrates after initial solidification or forming

processes are complete. These substrates are typically smooth and free of defects. Barcodes are typically read with the use of an imager and decoded using visual identification software. Barcodes have the capacity to contain a relatively large amount of alphanumeric data in a small space. Methods to cast barcodes have been proposed by Perma-Code [2] and Roxby [3], but expected performance of these methods has yet to be evaluated. The objective of this research is to establish a relationship between barcode performance and barcode design through modeling and experimentation. The understanding of this relationship between design and performance will aid in the implementation of cast barcodes within industry.

1.1 Industry Needs and Data Matrix Symbol Usefulness

The casting industry is characterized by the integration of labor and material to create a product with complex geometry that is of value to consumers. As is common with most production processes, variation separates initial castings from final castings. Secondary processes, such as grinding or machining, are necessary to transform these initial castings into final castings through further input of resources. Improvements to secondary processes are typically focused on automated systems for material removal, handling, and inspection. These automated systems require the identification of incoming product, which creates the need for unique part identification systems [4].

Product inventory is a critical process measure as it represents the financial investment necessary to account for inefficiencies and variation within a production system needed to maximize output of available capacity. The goal of profit seeking enterprises is to

create profit with the least amount of necessary investment. The level of work in process inventory is critical to determine a production system's throughput and cycle time [5]. The improvements of throughput and cycle time are important metrics to determine the reduction of waste, a key aspect of becoming a 'Lean' process. The gathering of data and information facilitates this measurement of process improvement.

Cast barcodes would serve as a unique identification of castings from the point at which they are cast. Cast barcodes would facilitate the gathering of information for process improvement. In other industries, unique identification of products has been supported by the use of printed labels such as data matrix symbols, allowing scanning technology to quickly and accurately read coded information. Similarly, in applications where printed media cannot withstand a harsh environment, data matrix symbols are formed into the product's substrate material.

1.2 Data Matrix Error Correction and Robustness

Data matrix symbols are a two dimensional array of nominally square modules with a finder pattern along the perimeter, as shown in Figure 1. Data matrix symbols are widely used as printed black and white labels and direct part marking systems. Materials such as metal and plastic can be impressed with symbols using various methods like laser etching, impressed dot peen, and ink printing. Data matrix is a symbology available in the public domain that allows scanning equipment manufacturers and producers of products requiring unique part identification to work together.
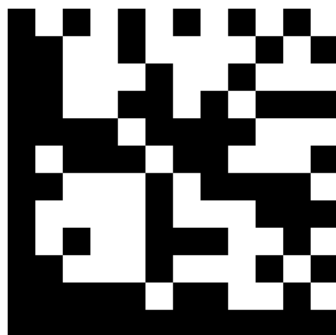
Figure 1: 12x12 module data matrix symbol coded '123456'

ISO 16022 is the specification used to describe data matrix symbol construction and the decoding algorithm. ISO 15415 describes symbol quality criteria and evaluation methods. Each symbol contains cells, referred to as modules, used to encode one bit of data and are usually square in shape. Modules are blocked together to create code words which are an intermittent level of coding between source data and graphical encodation in the symbol. The code words are placed in a data region array that is surrounded by a finder pattern with a quiet zone along all four sides.

The capacity of information contained in a symbol is dependent on its size ranging from 10x10 to 144x144 modules, not including rectangular symbols that employ interleaving, increasing data capacity further. Data matrix symbols using the type ECC 200 can encode up to 2,335 alphanumeric characters and 3,116 numeric characters. A 14x14 symbol contains eight data code words and ten error code words with a numeric capacity of 16 characters or ten alphanumeric characters.

An aspect of data matrix symbols that makes it particularly attractive to industry is the error correction feature. ECC 200 employs the Reed-Solomon error correction technique.

There are two types of defined errors that can occur when decoding a data matrix symbol: erasures and errors. Erasures are erroneous code words at known locations, while errors are erroneous code words at unknown locations. Erasures are symbol characters that are unscanned or otherwise not decoded and errors are symbol characters that are miscoded. The 14x14 symbol contains 18 codewords and can still be decoded when erasures and errors are less than seven and five, respectively. Meaning, 39 percent of symbol codewords can be obliterated and 28 percent can be misdecoded and the symbol will still decode successfully [5].

2. Literature Review

The standards related to data matrix symbol quality and other literature on methods proposed to cast data matrix symbols were used to guide development of this research. The measurement of symbol quality was an important aspect of the research objective to understand symbol performance, which is discussed in ISO 15415 [6].

2.1. ISO 15415 Data Matrix Symbol Quality Standard

As part of the research objective, the measurement of symbol quality was needed. Jangsombatsiri utilized ISO 15415 for the evaluation of data matrix symbols, which is a symbol grading method incorporated into verifier hardware available from most data matrix scanning equipment manufacturers. ISO 15415 data matrix symbol quality is expressed as an overall symbol grade. The overall symbol grade is the calculation of the lowest grade of the specific grading criterions: Decode, Symbol Contrast, Fixed Pattern Damage, Axial Nonuniformity, Grid Nonuniformity, Modulation, and Unused Error Correction [6].

An additional parameter is Print Growth, which tests that the graphical features of the symbol have not grown or shrunk from nominal so much as to hinder readability. ISO 15415 states Print Growth shall be an ungraded measure of quality. The scanning software used in this research for quality evaluation did use Print Growth as a part of the final grading criteria and was treated likewise by Jangsombatsiri. This is of particular interest because Jangsombatsiri found Print Growth and Symbol Contrast to be the grading criteria that most affected overall symbol grade [7].

2.1.1. ISO 15415 Symbol Contrast Calculation

In previous data matrix symbol research, Symbol Contrast was shown to be a critical symbol performance factor. ISO 15415 defines the procedure for calculating Symbol Contrast. The procedure includes the identification of a reference grey-scale image of the symbol and inspection area by applying the Reference Decode Algorithm defined in ISO 16022. Reflectance values for all pixels in the reference grey-scale image are inspected and the highest and lowest values are selected for R_{max} and R_{min}, respectively. In printed applications, Symbol Contrast serves as a control of the measure of the difference between the reflectance values of the inks used to print a symbol. In other words, if a printer begins to deplete its ink supply, symbols with insufficient printed ink will be rejected due to poor Symbol Contrast grade. For direct part marking applications, Symbol Contrast quantifies the ability of the surface to deflect or dampen the reflection of incident light as measured by the imager. Symbol Contrast is calculated as:

$SC = R_{max} - R_{min}$

Table 1 contains grading thresholds for Symbol Contrast, which is graded using a four point scale:

Table 1: Symbol Contrast grading thresholds as defined in ISO 15415.

Symbol Contrast	Grade
≥ 70 %	4
≥ 55 %	3
≥ 40 %	2
≥ 20 %	1
< 20 %	0

2.1.2. ISO 15415 Print Growth Calculation

Print Growth is the measure to which contrast marks appropriately fill their module boundaries and is a critical factor of symbol performance. To calculate Print Growth, module boundaries are determined by applying the Reference Decode Algorithm to the binarized symbol image, as defined in ISO 15415. If marks are small relative to module boundaries, Print Loss will be excessive. However, if marks are large relative to module boundaries, Print Growth will be excessive. The spacing between marks will also affect Print Growth and Loss.

ISO 15415 indicates Print Growth shall not be a graded parameter but should be reported as an informative measure for the purposes of process control. Because Print Growth is not a graded measure in ISO 15415 there are no defined grade thresholds. The grade thresholds in Table 2 are obtained from the software program utilized for this research [7]. Previous research on Data Matrix symbols also treated Print Growth as a graded parameter, which motivated its calculation for this research [8]. Print Growth units are expressed in terms of module width. A positive value for Print Growth corresponds to a mark that exceeds the established module boundaries, while a negative Print Growth value is Print Loss, which represents marks that do not completely fill the module boundary space. The ideal value for Print Growth is zero. By applying the Reference Decode Algorithm, the module width for a symbol is determined, which is then used to calculate Print Growth values and symbol grade. An illustration of Print Growth and Loss marks and 'ideal' marks are shown in Figure 2.

Table 2: Grading for Print Growth.

Print Growth (x)	Grade
-0.50 ≤ x ≤ 0.50	4
-0.70 ≤ x < -0.50 or 0.50 < x ≤ 0.70	3
-0.85 ≤ x < -0.70 or 0.70 < x ≤ 0.85	2
-1.00 ≤ x < -0.85 or 0.85 < x ≤ 1.00	1
x < -1.00 or x > 1.00	0
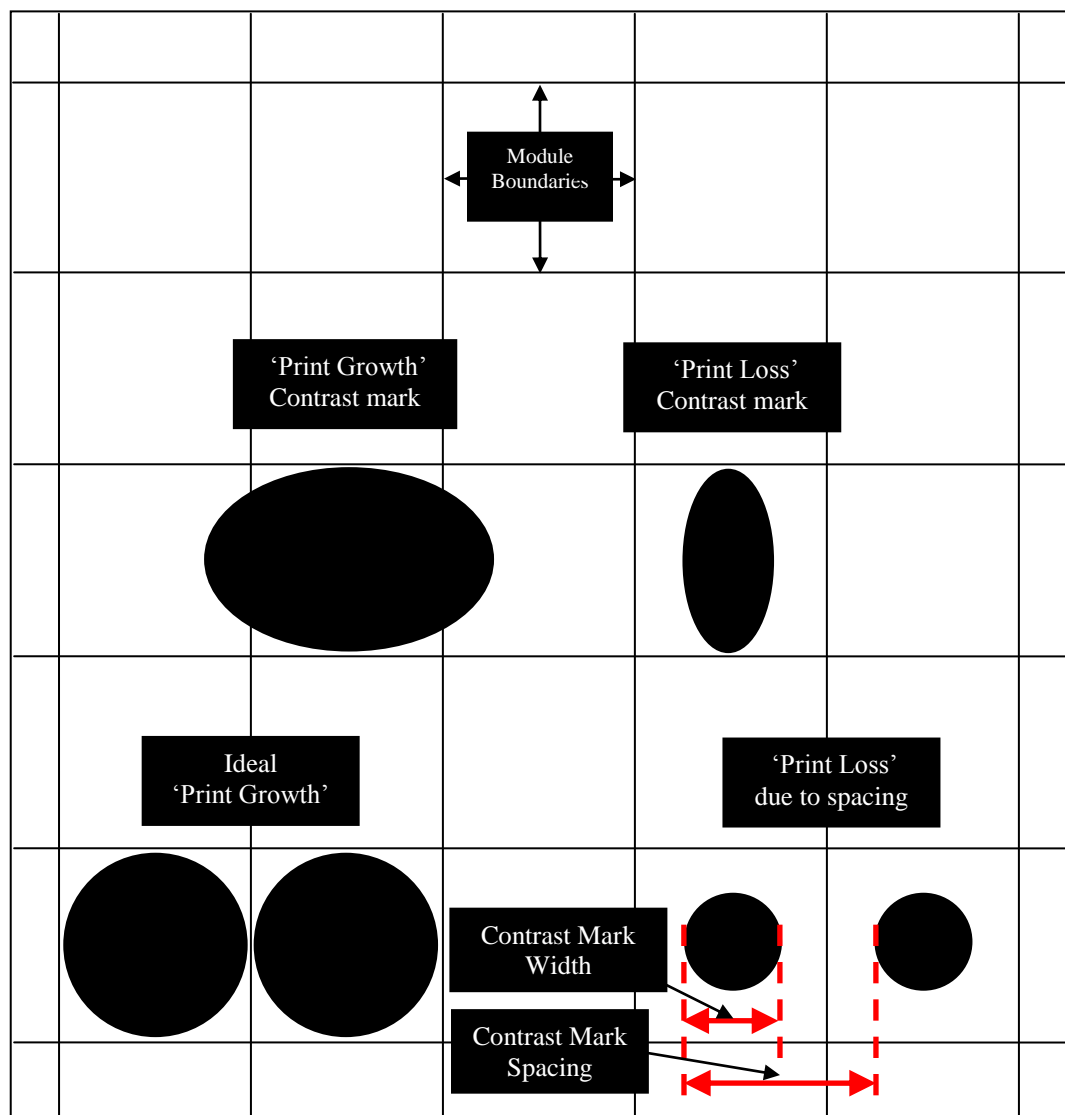
Figure 2: Print Growth and Loss illustration with views of ideal contrast marks and the effect of contrast marks spaced far apart. Ideal marks are those that extend up to module boundaries.

2.2. Cast Data Matrix Methods Overview

Cast data matrix research was influenced by the previous work relating to laser etched data matrix symbols. The method employed by Jangsombatsiri to determine symbol performance was utilized with cast data matrix symbol research. In addition, proposed cast data matrix methods were reviewed and used as motivation of the feasibility of future cast data matrix symbols, as well as indicated an absence of cast symbol performance data.

2.2.1. Laser Direct-Part Marking of Data Matrix Symbols on Carbon Steel Substrates, Jangsombatsiri and Porter 2007

The performance criteria Print Growth and Symbol Contrast were used in the research by Jangsombatsiri to evaluate symbol performance. Jangsombatsiri's use of laser direct part marking is similar to the approach of cast data matrix symbols. The objective of Jangsombatsiri and Porter 2007 was to establish a relationship between critical laser parameters and the resulting performance of the data matrix symbols. Over 100 data matrix symbols were marked with a laser onto two different metallic substrates at differing levels of laser parameters. The symbols were evaluated for quality using ISO 15415. Statistical analysis was then completed to identify the critical parameter combination necessary to maximize performance and develop a robust marking process.

In the final conclusion, factors that affected overall symbol grade were determined to be Print Growth and Symbol Contrast. Print growth was improved after a specialized symbol cleaning process was employed, which removed a laser residue resulting from the

marking process. After the cleaning process, symbol contrast was the single factor affecting final symbol grade, stating "additional research outside of the scope of this thesis is necessary to better understand this phenomenon." [7]

2.2.2. NASA Technical Handbook for Data Matrix Direct Part Marking

The NASA Technical Handbook for Data Matrix Direct Part Marking provides guidance for using permanent direct part marking methods and techniques to apply data matrix symbols safely to products. A section of the handbook refers to a method for sand casting processes. It was proposed that the process can be adapted to apply data matrix symbols using an Yttrium Aluminum Garnet (YAG) laser configured for deep-laser engraving to cut a symbol directly into a sand mold, which then would be cast in metal. The laser was used to produce symbols of varying sizes, depths, or shapes in the sand mold. It was suggested in the NASA handbook the contrast mark shapes would theoretically reflect light away from the reader lens, creating the contrast needed for successful reading [9]. Figure 3 shows the depiction of the laser beam path onto the sand surface used to create the mark geometry. Figure 4 shows the resulting casting being scanned where light is theoretically directed away from the imager by the cast mark geometry. An aluminum casting that utilized a sand mold with laser engraved data matrix symbol is shown in Figure 5.
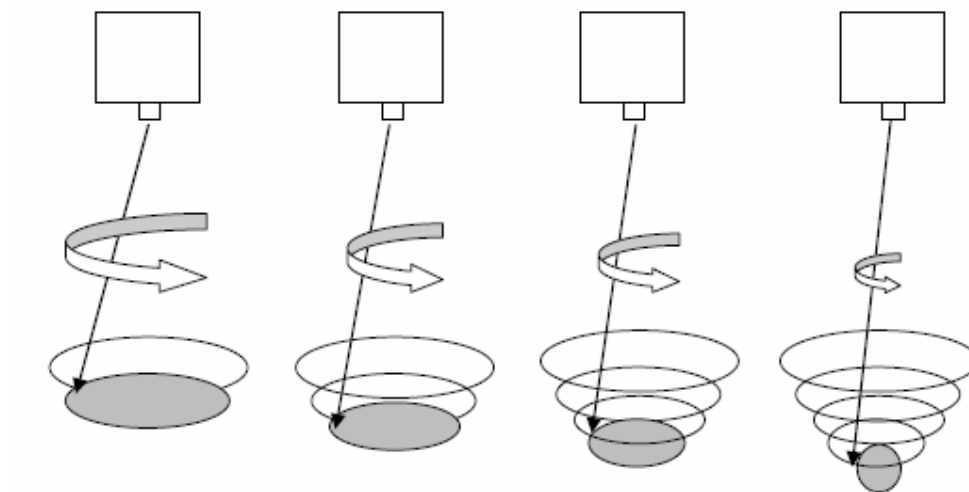
Figure 3: Laser path over sand core surface creating conicular module geometry [9].
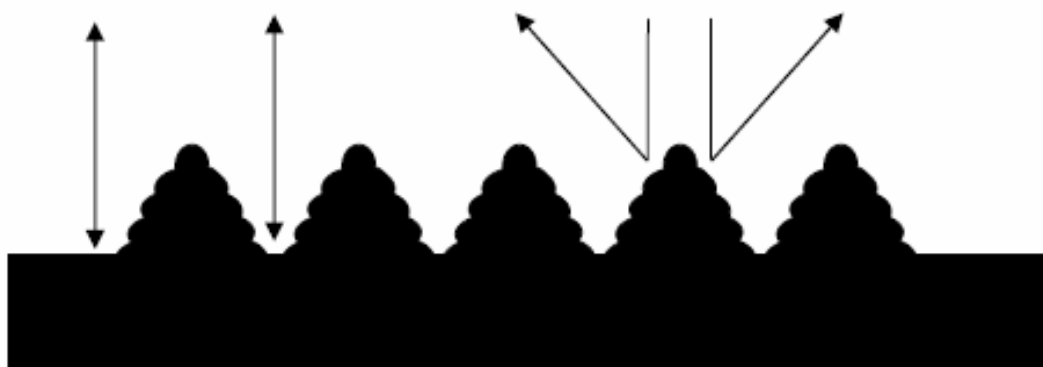
Figure 4: A casting with a data matrix symbol contrast mark deflecting light from imager [9].
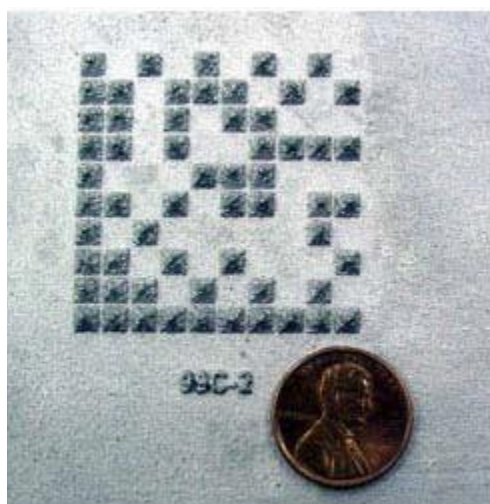
Figure 5: Aluminum data matrix symbol casting using a laser etched sand mold [9].

The laser engraving process was developed by RVSI, which is a now defunct company that focused on research applications for direct part marking technologies. The unpublished report of the project claims raised symbols produced in the study "exceeded expectations" and demonstrated that the method may prove useful to industry [3]. Absent from the study were results indicating the evaluation of cast symbols using a grading standard such as ISO 15415. Symbol Contrast was a factor that was emphasized as being a major asset to the method, but no symbol grades were presented to verify this conclusion.

2.2.3. Stencil Cast Symbols

A commercially available method of creating cast data matrix symbols utilizes ceramic stencils to create symbol geometry. The stencils are fabricated using a precise water jet cutting method to shape ceramic material. Though there has been no development with the method in the past five years, the stencils are available for use in foundries. The basic premise of the use of stencils is that the material used to create the stencil is resistant to combustion and abrasion. The stencils are affixed inside a mold prior to pouring. After the mold is poured, a raised data matrix symbol with square modules is created on the cast surface.

The available literature from the product supplier does not provide ISO 15415 results to verify the performance of cast data matrix symbols using the method. Figure 6 shows cast data matrix symbols created using stencils, which have been treated with paint and chemical etching to increase Symbol Contrast. One could infer the need to treat the

symbol indicates is a lack of Symbol Contrast, but no symbol grading data is available to make a determination.
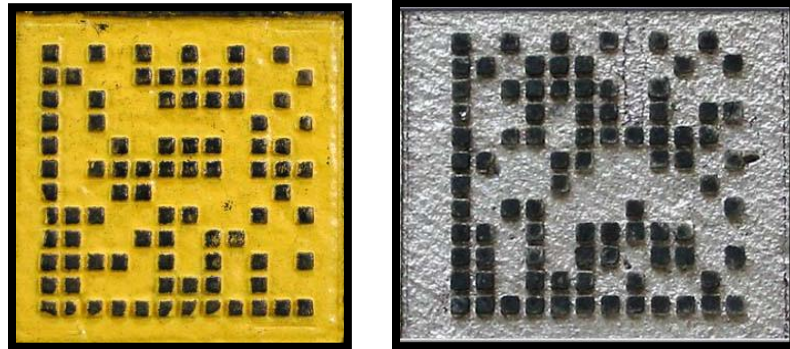
Figure 6: Enhanced Symbol Contrast with the use of paints and chemical treatment [6].

2.2.4. ISU Aluminum Feasibility Trials 2006

An experimental project was conducted by the Iowa State University Industrial Engineering department in 2006, which set out to determine the feasibility of drilling molds with geometry to create Bump modules [10]. The goal was to cast drilled symbols in aluminum and compare results to cast data matrix symbols created using a commercially available ceramic stencil.

The approach to drilling a symbol into sand was crude, utilizing a Dremel tool and a data matrix symbol pattern to position the tool. The result was an approximately two inch square, 10x10 data matrix symbol with approximately 0.250 inch diameter contrast marks as shown in Figure 7. After the symbols were created and cast, they were read with a vision system. An optimized setup of the vision was required to allow the symbols to read. The setup was developed through a process of trial and error, resetting the light angle and adjusting light settings until the majority of the symbols read.

Figure 7: ISU group project cast symbol. Shown is a cast symbol that was readable.

The project result was that 'nearly every' symbol produced using the crude method decoded. The conclusion was that it was feasible to produce decodable symbols using a crude method. It was further concluded that data matrix symbol error correction provided a high level of robustness that aided in the positive results and if greater production control was achieved better results might be possible. It was hypothesized that surface finish was a critical factor in symbol readability, but this was not a factor that was controlled for analysis.

3. Experiment One and Two

The following experimentation was directed by the findings from previous work. From the literature review it was concluded:

1. Cast aluminum symbols that decode were feasible

2. ISO 15415 grading is essential in determining the performance of cast symbols

3. Several symbol casting methods have been proposed, but no symbol grading results have been published

These outcomes led to the series of experiments contained in this work. Each experiment was based on results and conclusions of the literature or prior experiments. Table 3 is an aid in understanding of the general direction of the research.

Table 3: An overview of experimentation for the research is shown in the table below.

Experiment Title	Variable	Replications
Experiment One	Power drill machined Bump marks with three mark diameters and two mark depths	Six total symbols
Experiment Two	CNC drilled and pattern molded Bump marks with coating applied to half	36 total symbols
Experiment Three	Molded dimple marks	12 total symbols
Experiment Four	Bump vs. Dimple at various light angles	Two total symbols, four light angles
Experiment Five	Fabricated test modules with a range of dimple diameters and spacing, surface roughness and light angle	36 total modules pairs on four surface roughness substrates, three levels of module spacing, three mark diameters, and four light angles.

The methods discussed in the literature review used a cast data matrix symbol design that employed raised mark geometry. Raised contrast marks form a 'bump' on the cast surface and will be referred to as Bump contrast marks for the remaining discussion. A fundamental aspect of Bump modules is they can be produced in the mold by employing

sand removal techniques, as was done in the laser engraving process. This procedure lends itself well to creating simple processes for sand removal such as drilling sand molds to create mark geometry. Also, bumps are a preferred geometric feature because they will not form stress risers at the casting surface. Preliminary experimentation focused on drilling sand molds as a means to create mark geometry.

3.2 Experiment One: Steel Feasibility Trial

The motivation for evaluating the feasibility of symbols cast in steel was that in comparison to aluminum, steel has greater density and higher melting point leading to relatively high levels of mold surface abrasion. It was inferred this abrasion would affect symbol performance. Therefore, if a readable symbol is produced in steel, other materials with less density and a lower melting point would likely experience success. Furthermore, an experiment goal was to determine the smallest decodable symbol using the drilling method.

To produce steel casting symbols, a similar method, as described in the aluminum feasibility trials, was used to produce cores for the steel feasibility trials. A sand drag without geometry was obtained from the University of Northern Iowa Metal Casting Laboratory. Jigs for machining the drag were created, shown in Figure 8. Paper patterns were adhered to the jigs to indicate the location of holes to be drilled into the sand.
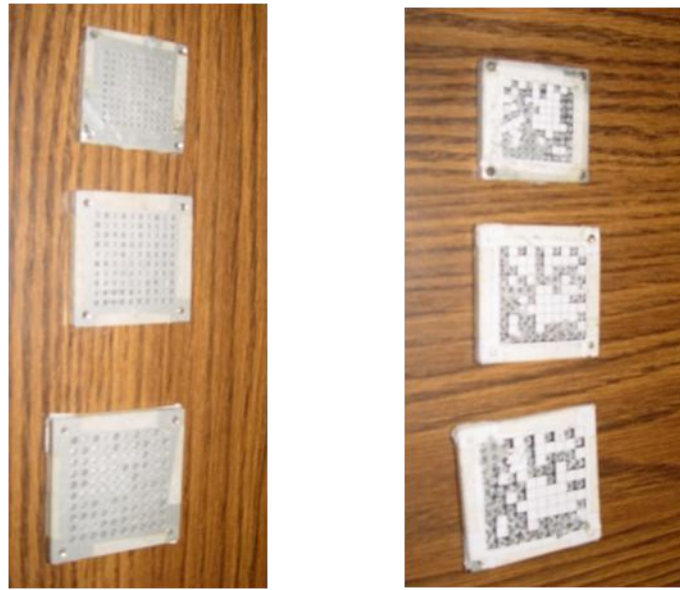
Figure 8: Jigs used to machine sand drag with Data Matrix symbol for Experiment One. Left image shows holes in jig, while the right image shows the symbol indicated location of contrast marks that guided the drilling process.

A power drill was used in conjunction with the jig to create holes in the sand drag. Holes were drilled at two depths, 0.125 and 0.250 inches, to create mark geometry. Three module diameters were created: 0.250, 0.125, 0.0625 inches to create three symbol sizes. Once the sand drag was completely drilled with the symbols, a cope was placed on top which created the casting cavity, as shown in Figure 9. The sand from the center of the cope was removed leaving the mold assembly top open, resulting in an approximately prismatic shape casting. A duplicate mold assembly was created using the same procedure. The drag and cope were transported to a steel foundry facility and poured using a 'tea pot' pouring crucible. The resulting castings were approximately 10 inches by 14 inches by 2 inches in size.
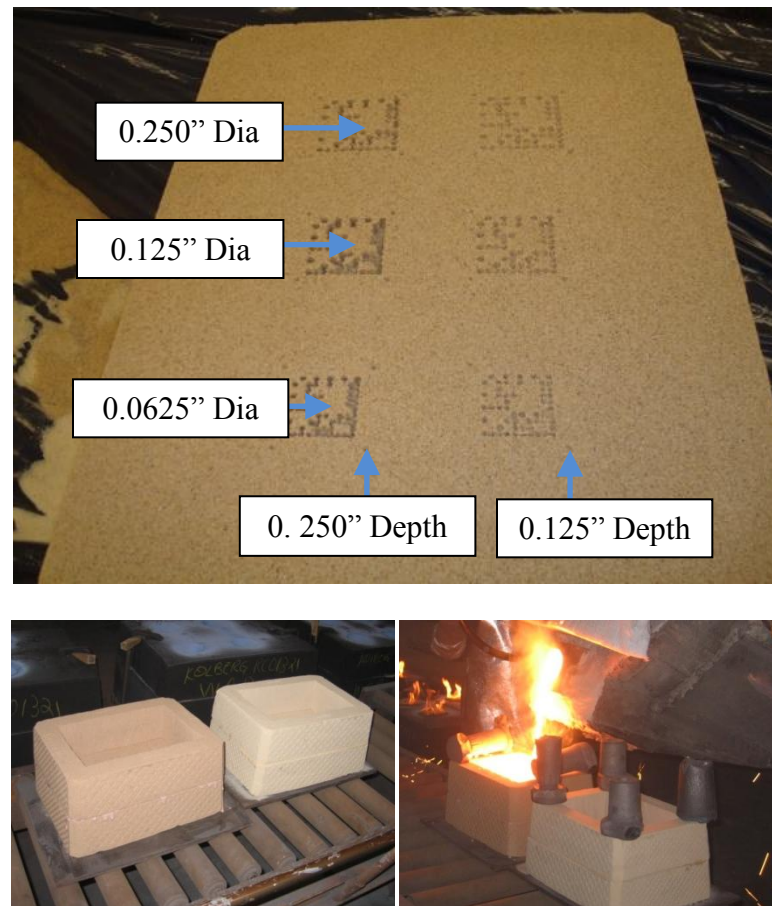
Figure 9: Drag machined with Data Matrix symbols. Cope and drag assembled together prior to being poured.

The experiment objective was to determine the smallest decodable symbol that could be cast. The hypothesis was that disruption from surface roughness would cause small modules to not be discernable by imaging systems. The largest steel symbol cast was equal to those cast in the aluminum feasibility trials. Figure 10 shows the casting produced with each symbol size and depth.
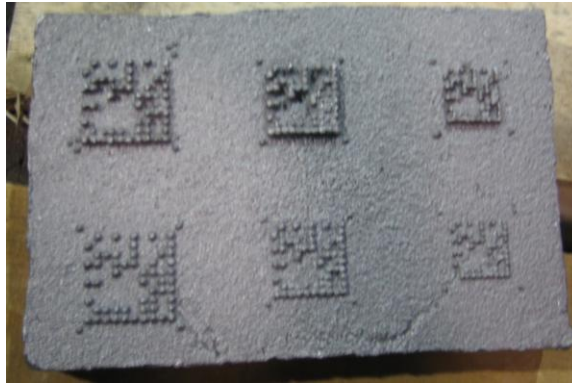
Figure 10: Steel casting with six factor combinations.

After the castings were poured they were knocked out of sand and shot blasted to remove remaining sand. A single steel casting was sent to a vision system vendor for decoding. Figure 11 summarizes the results of the steel cast data matrix symbol analysis. The 0.250 inch diameter symbols both decoded successfully.   Neither symbol with 0.125 inch diameter symbols read.   One of the two smallest module diameter symbols decoded indicating it is feasible to decode cast data matrix symbols with module diameters as small as 0.0625 inch.
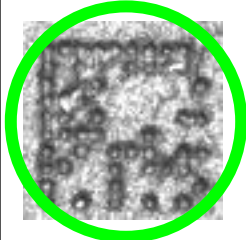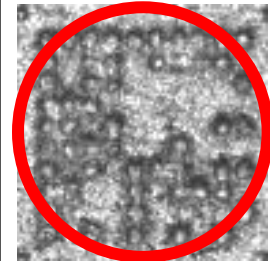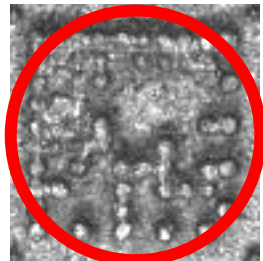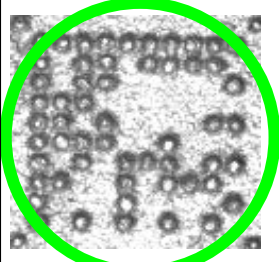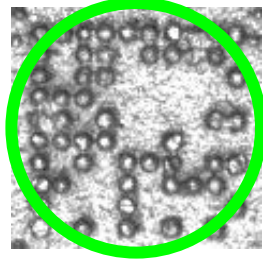
Depth: 0.125 inch Diameter: 0.0625 inch Decode: Yes Observation: Mostly connected modules	Depth: 0.250 inch Diameter: 0.0625 inch Decode: No Observation: High level of erosion
Depth: 0.125 inch Diameter: 0.125 inch Decode: No Observation: Partial obliteration of	Depth: 0.250 inch Diameter: 0.125 inch Decode: No Observation: High level of erosion
Depth: 0.125 inch Diameter: 0.250 inch Decode: Yes Observation: Well developed modules	Depth: 0.250 inch Diameter: 0.250 inch Decode: Yes Observation: Well developed modules

Figure 11: Steel casting symbol feasibility results.

As stated initially, determining the feasibility of cast data matrix symbols in steel was the objective of the trial. Three of the six symbols decoded, including one of the smallest symbols cast. The inferred factor leading to the 0.125 inch symbols not decoding was the proximity of the symbols in the mold which led to excessive erosion where the first metal

poured came in contact with the mold surface. The location likely increased the severity of erosion due to the heat and force on the mold assembly drag from the poured metal.

The conclusion was that it was feasible to cast data matrix symbols in steel and that symbols with module diameters at least as small as 0.0625 inch could feasibly be produced. However, the methods used in the experimentation to produce the cast symbols were relatively crude in design. The effect of improved control on decode rate and symbol grading over several replications was still unknown, which was a focus of future experimentation.

3.3. Experiment Two: Aluminum Cast Symbol Performance Study

Previous experimentation and Experiment One indicated that symbols in aluminum and steel could be cast using a drilling production method. The results of the steel trial were that symbols with contrast marks as small as 0.0625 inches could be read, but the expected performance and effect of improved process control was unknown. Experiment Two focused on investigating production methods that would provide improved control of the geometric shape of the symbol features, while establishing an expected level of performance from cast symbols.

A preliminary experiment was planned with the objective of improving production process control in the experiment, while measuring symbol grading performance and symbol decode rate over several replications. The hypothesis of the ISU aluminum feasibility trial was that surface roughness affected symbol performance. This theory was

evaluated as a factor using mold coatings, which is a common method to improve casting surface finish. Coatings contain small grain silica or other media that bond to the mold which functions as a substrate material. Also, it was observed that the drilling process left a less smooth mold surface compared to adjacent mold surface. A method to produce symbols without drilling that replicated the adjacent mold surface was incorporated into the experimentation.

3.3.1. Experiment Two Overview

In Experiment One, drilling was the process used to create mark geometry. The drilling process was controlled by a human operator, which was viewed as a source of variation that could be removed. To remove this variation in the drilling process, the introduction of CNC controlled drilling replaced the human controlled drilling in the experimentation. The CNC tool path was programmed so a drill tool plunged into a sand core to create the Bump contrast geometry, replicating the path previously used by the human operator.

It was observed that drilling sand to create geometry resulted in an increase in mold surface roughness. An alternative to creating drilling symbol geometry was incorporated into the experimentation. It was observed in Experiment One surfaces adjacent to the drilled marks, created by the pattern, left a smooth mold finish, as illustrated in Figure 12. From this observation, it was hypothesized that by using a pattern to create contrast marks, sand grains are uniformly placed along the pattern surface to create an improved surface finish than that created by the drilling process.

Figure 12: Cross sectional view of a drilled sand mark. The drilled surface is relatively rough compared to the molded core surface. Using pattern surface symbol geometry to create marks was used in as an experimental factor.

A pattern with symbol geometry was needed to replicate the surface finish condition of the pattern surface observed in Experiment One. The process used to create a symbol pattern is shown in Figure 13. The process began with creating a solid CAD model of the symbol pattern. The model was used to generate tool paths for a CNC milling center. A wax block was machined with the symbol geometry, which was then used to form a urethane pattern that was the reflection of the original wax geometry. To replicate the intended Bump geometry, urethane was poured over the original urethane pattern to again create a reflected geometry with Bump marks. This final urethane pattern was fabricated with sides to create a complete core box. Using the no bake core making process, silica sand bound with phenolic urethane resin was placed into the core box containing the symbol pattern to create the symbol sand core.
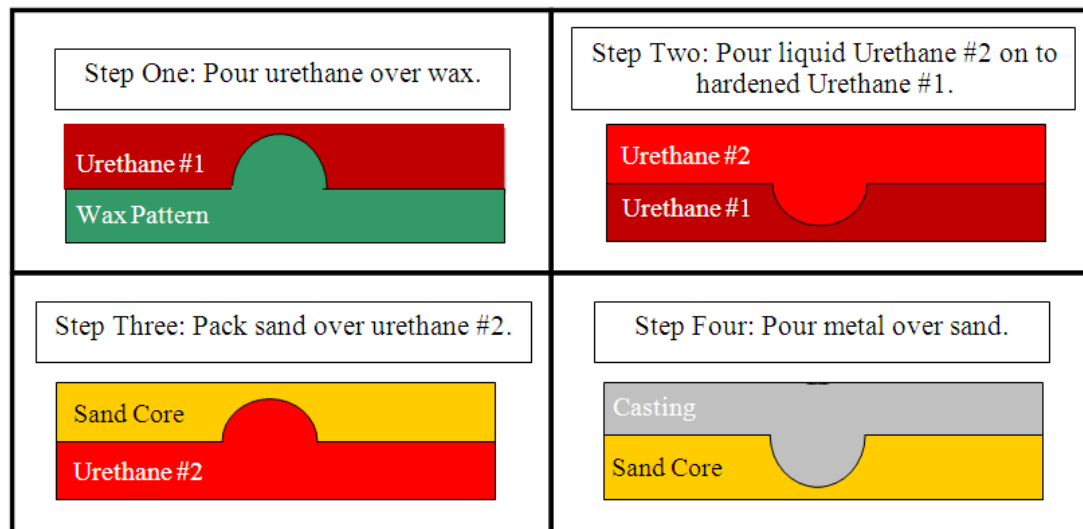
Figure 13: Pictorial representation of experimental pattern development.

Figure 14 shows the CNC machined wax block, urethane pattern and core box, and resulting sand core used to produce the experimental sand casting. The final sand core had a 12x12 symbol with 0.125 inch hemispherical Bump contrast marks. The designed spacing between Bump modules was 0.03125 inches, which was the smallest possible spacing due to tooling limitation.
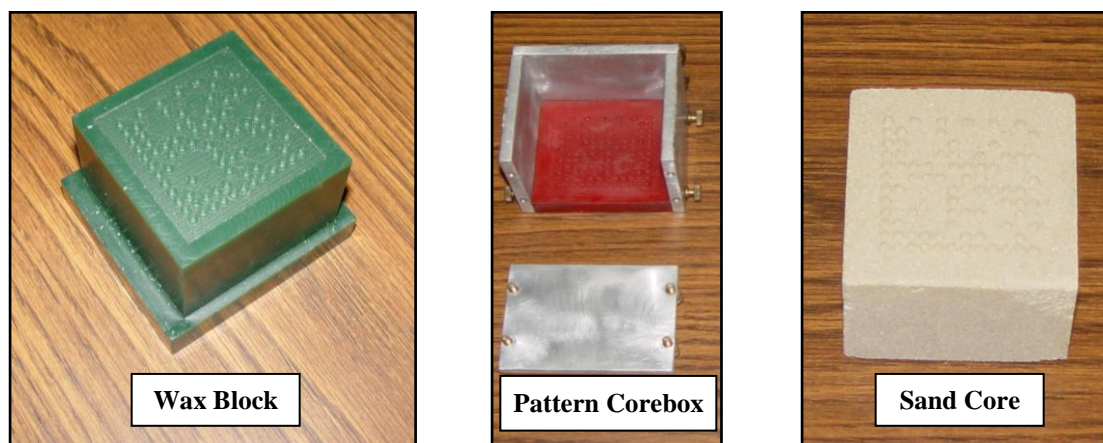
Figure 14: Overview of method used to create symbol sand cores.

A casting was created to administer the experimental design that incorporated the sand cores with symbols. The casting was designed to utilize twelve individual symbol cores placed in the mold cavity. The coating, CNC machined, and symbol pattern treatment combination sand cores were randomly placed in the mold cavity to prevent bias in the results. Three castings were produced with 12 symbols on each casting. Figure 15 shows the experimental casting mold assembly, with symbol sand cores inserted. The cores sprayed with coating are have a blue color. A cope was placed atop the drag to close the mold before pour.

Figure 15: Experimental casting drag setup with symbol sand cores inserted into drag.

After the mold containing the symbols was poured the rough casting was degated and sand blasted. The resulting casting was prismatic in shape with nominal dimensions of approximately 11 inches long, 8.25 inches wide and 0.5 inch depth, shown in Figure 16.
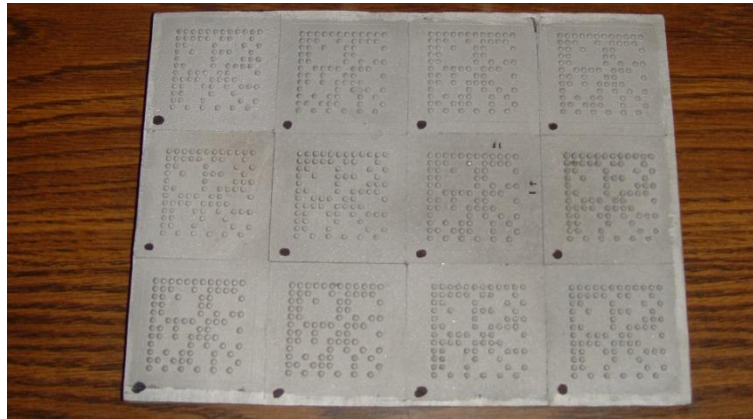
Figure 16: Resulting casting incorporating machined and pattern mark geometry and coatings.

From the symbol pattern, 18 symbol sand cores were created, while an additional 18 cores were CNC machined. Coatings were applied to half of each core type as final factor. 36 total cores were placed in three castings. Table 4 summarizes the experimental design used in the preliminary experiment.

Table 4: Preliminary experimentation design factors, emphasis on surface roughness control.

Contrast Mark Production Factors	Coated	Uncoated
Machined Geometry	9 Replications	9 Replications
Pattern Geometry	9 Replications	9 Replications

The symbol performance analysis was performed using a Cognex camera and DVT Intellect software. The grading procedure followed the procedure described in ISO 15415. If the decode of an image was unsuccessful, a grade of zero was awarded. Figure 17 is a screen capture of DVT Intellect analysis of a cast symbol.
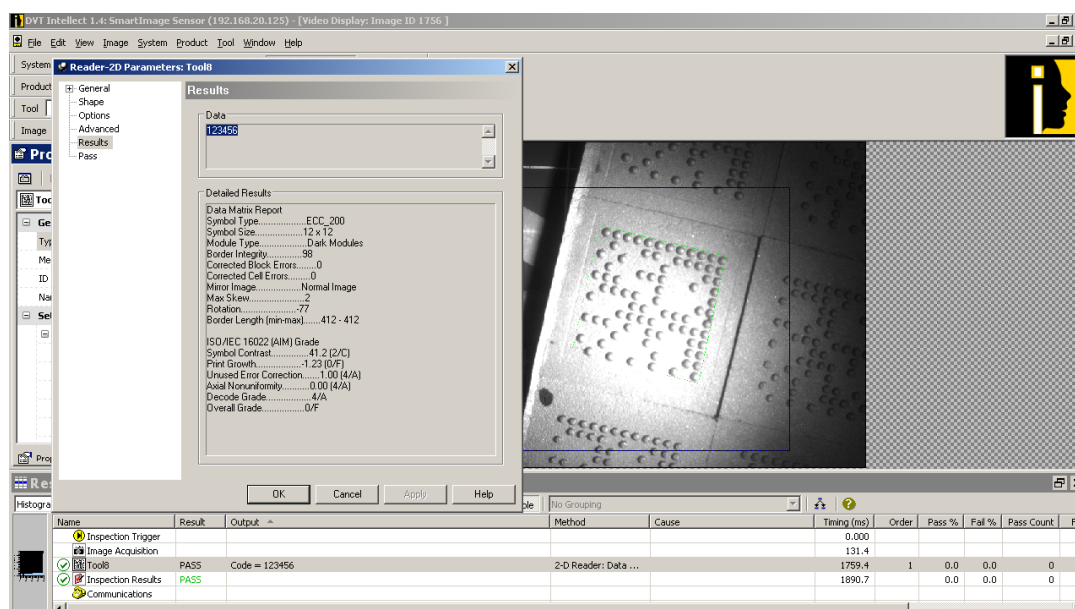
Figure 17: DVT Intellect software screen capture.

3.3.2 Experiment Two Results

After analysis was completed, the results were tabulated. To determine the impact of each factor, the average symbol grade and read rate for each factor combination was calculated. Read rate was calculated as the percentage of total decodes of all acquired symbol images. The treatment combinations are summarized in the Table 5.

Table 5: The treatment naming convention for this experiment for the two factors is shown as four treatment combinations.

Treatment Name	Description
Machined, Coating	CNC machined cores with coating applied.
Machined, No Coating	CNC machined cores with no coating applied.
Pattern, Coating	Cores with pattern mark geometry with coating applied.
Pattern, No Coating	Cores with pattern mark geometry with no coating applied.

The average symbol grade for each factor combination is shown in Table 6. The highest average grade for any factor combination was 'Pattern, No coating' averaging a 0.378 grade out of 4.000, while 'Pattern, Coating' averaged lowest grade at 0.133. The average

of all symbol grades was 0.233 out of 4.000, which equated to a failing grade for the ISO

15415 grade criteria.

Table 6: Preliminary experiment results by factor combination with symbol grades.

Treatment	Average Symbol Grade
Pattern, No Coating	0.378
Machined, No Coating	0.222
Machined, Coating	0.200
Pattern, Coating	0.133
All Symbols	*0.233*

Figure 18 is a plot of the average symbol grade result for each factor combination. The

machine symbol averages averaged symbol grades relatively close together. The molded

symbol grades have a wider difference in grade average. The difference between the two

averages for each production method was the application or absence of coating, a step

that provided improved surface finish.
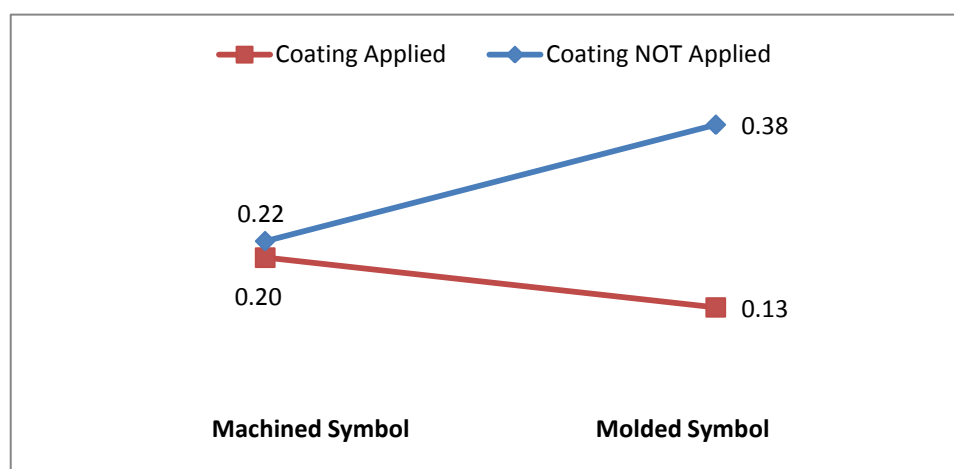
Figure 18: Plot of results for average symbol grade factor combination values.

Analysis of variance was calculated to determine the effects of the controlled factors,

shown in Table 7. The two factors evaluated were the application of coatings to the

symbol cores and the method used to produce the symbols. The ANOVA analysis

included the calculation of the F ratio to determine the effect of each factor. The F distribution table was consulted to determine the F value threshold to test the null hypothesis. The threshold value was determined to be 4.17 at 0.05 significance level [11]. If the F ratio calculated from the experimental data was greater than the F threshold value, statistically significant effects are considered to be present within the variance. In this case, the F ratios calculated for coating, symbol production method, and the effect of the interaction of both factors were not statistically significant. Therefore it was concluded the null hypothesis was correct.

Table7: ANOVA results for Experiment Three. The critical F value was determined to be 4.17, indicating the null hypothesis was not rejected.

Source of variation	Sum of squares	Degrees of freedom	Mean square	F
Coating	0.160	1	0.160	3.39
Method	0.018	1	0.018	0.38
Interaction	0.111	1	0.111	2.35
Error	1.511	32	0.047	
Total	**1.800**	**35**		

In addition to symbol grade, read rate for each factor combination was also a calculated. Table 8 shows the results for symbol read rate for each factor combination. 'Pattern, Coating' appeared to have the highest read rate at 71 percent of images decoding properly, while 'Machined, Coating' had the lowest read rate at 47 percent of images decoding properly. The average for all symbol images was 57 percent read rate. Industry would likely require a read rate that exceeds 90 percent to be considered a viable part tracking system.

Table 8: Average symbol read rate for each factor combinations.

Treatment	Read Rate
Pattern, Coating	71%
Machined, No Coating	58%
Pattern, No Coating	51%
Machined, Coating	49%
All Symbols	*57%*

As was done with the symbol grade averages, the read rate averages were plotted, shown in Figure 19. It can be seen that read rates for machined symbols were generally lower than the molded symbols. The application of coating gave mixed results showing that for machined symbols the uncoated cores read more often, while for molded symbols the coated symbol read most often.
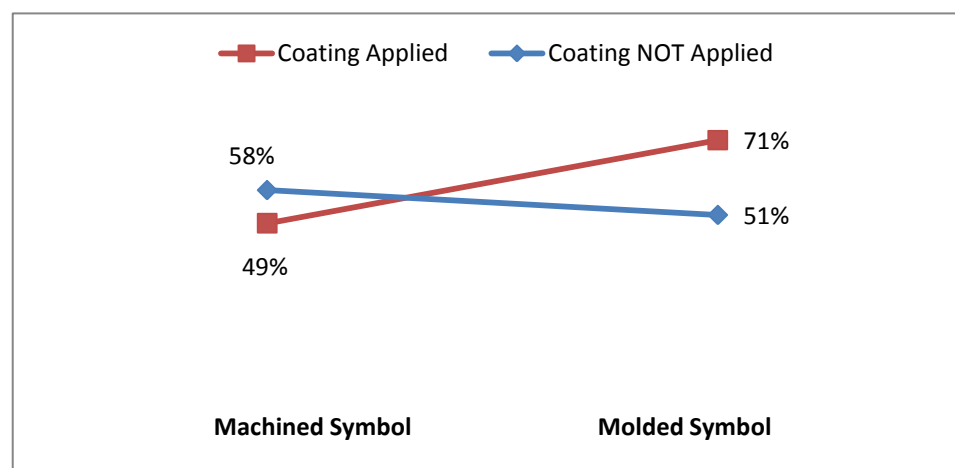
Figure 19: Plot of results for average factor combination read rate values.

The analysis of variance for read rate percentage was also calculated. The results shown in Table 9 indicate, again, the F ratio results are not sufficiently high enough to conclude statistically significant effects were present. This result agrees with the data found in the symbol grading results that either experimental factor was not statistically significant in the experimental result.

Table 9: Read rate ANOVA table of the experimental results. The F threshold value was found to be 4.17, therefore it was concluded effects were not statistically significant.

Source of variation	Sum of squares	Degrees of freedom	Mean square	F
Coating	0.028	1	0.028	0.51
Method	0.054	1	0.054	1.00
Interaction	0.188	1	0.188	3.45
Error	1.742	32	0.054	
Total	**2.012**	**35**		

The results of the experimentation indicate that effects from coating or symbol production method alone do not significantly affect the result of symbol grade or read rate. It was observed that the highest symbol grade factor combination was the molded symbols with no coatings applied. Of all factor combinations attempted, this would be the recommended procedure if the objective was to maximize symbol grade. The factor combination of molded symbol with coatings gave the highest average read rate of all procedures in the experiments, indicating that to maximize read rate, this procedure would lead to the best result of 71 percent read rate.

To improve understanding of the symbol grade results, further analysis was performed. For each grade calculation, lowest grade criterion dictates the final symbol grade. The scan grades were evaluated to determine which individual grade criterion most often the lowest or 'constrained' the final grade. The percentage of instances each criterion constrained the overall symbol grade was calculated. The grade criterion Print Growth was found to be the constraining criterion in 76 percent graded images, followed by Symbol Contrast in 15 percent of graded images. The complete breakdown of constraining grade criterions is shown Figure 20.
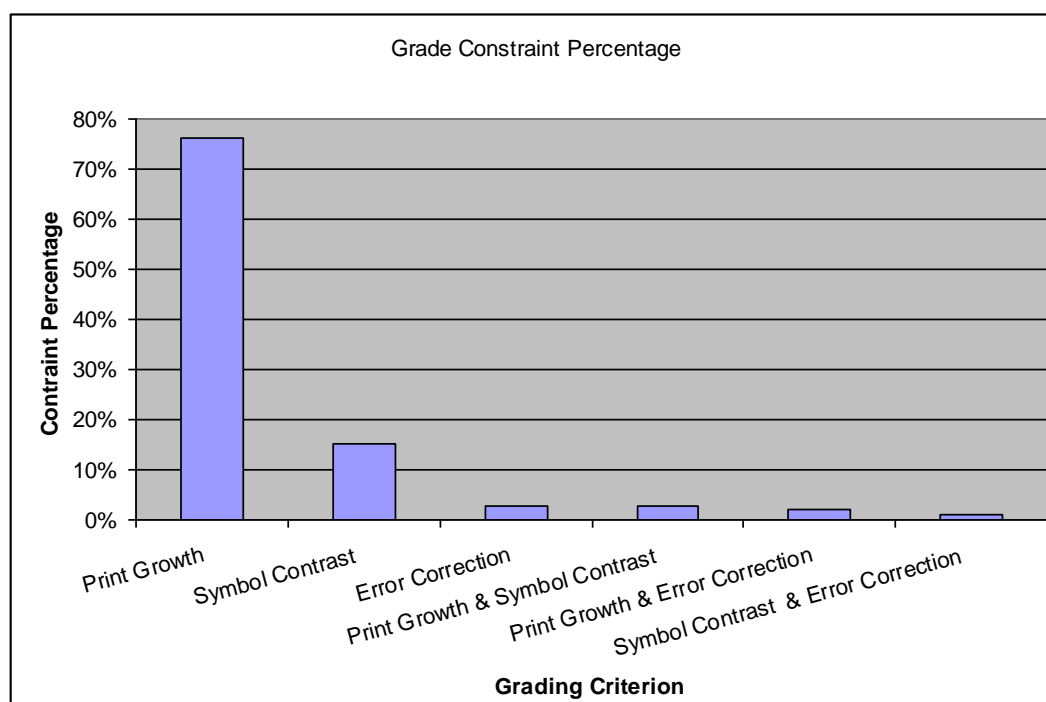
Figure 20: Grade constraint breakdown by criterion indicating Print Growth and Symbol Contrast are major constraints of final symbol grade.

3.3.3. Experiment Two Discussion

Once the experiment results were calculated, the implications of the information were considered. The ANOVA calculations indicate that for both symbol grade and read rate there were no statistically significant factors observed in the experimentation. The factor combination that resulted in the highest symbol grade was a coated core using a pattern to create symbol geometry at 0.378 out of a possible 4.000, a failing average symbol grade. While the factor combination that resulted in the highest read rate was a core not coated made with a pattern for create symbol geometry at a read rate of 71 percent, below the 90 percent read rate likely required by industry.

The primary goal of implementing cast symbols is to achieve high readability. Before experimentation was executed, 'Machined, coated' was viewed as most practical core production method, but yielded a failing average grade and read only 58 percent of the time. This percentage is also not a sufficiently high enough to be considered the factor combination feasible for industry. Surface roughness was hypothesized to be a critical factor towards symbol performance, but the results indicated that core coatings did not have a statistically significant effect on symbol grade or read rate.

The analysis of the constraining grade criterions indicated that Print Growth and Symbol Contrast most often scored the lowest value that constrained overall symbol grade. As previously discussed, Print Growth measures contrast mark size and location within the module boundaries. It was hypothesized that Bump modules rely on three phenomena to create contrast marks in an acquired image: deflected light from a directional light source, absorption of light, and shadows cast by directional light. Deflected light works best with smooth, mirror surfaces, which uniformly directs light away from the imager in contrast mark symbol regions and reflects light in all others as previously shown in Figure 4. Absorption of light occurs when a surface does not reflect light, but rather dampens its reflection, as previously shown in Figure 6. The application of black, contrasting materials or paints has been used to accomplish this task as do greater surface roughness in contrast mark locations.

The determination that Print Growth was the constraining grade criterion indicates that contrast marks were extending beyond symbol boundaries. When light is incident on a

Bump mark, it casts a shadow in the direction of the light path, which it was inferred to cause the high levels of Print Growth scores. A mark geometry that improves containment of shadows may improve Print Growth performance. The dot peen data matrix symbol is a widely used direct part marking method, which uses an indenter to impress mark geometry into the substrate material. Dot peen symbols use indentions to contain shadows within module boundaries. Figure 21 is a typical dot peen symbol marked onto a metal substrate. The dot peen mark geometry is approximately an inverted hemisphere. The following motivation was used for the planning of a future experiment:

(1) Shadows may be responsible for the excessive Print Growth values seen in Bump marks.

(2) More accurately placed shadows within module boundaries may lead to improved results, using the same approach as dot peen data matrix symbols.
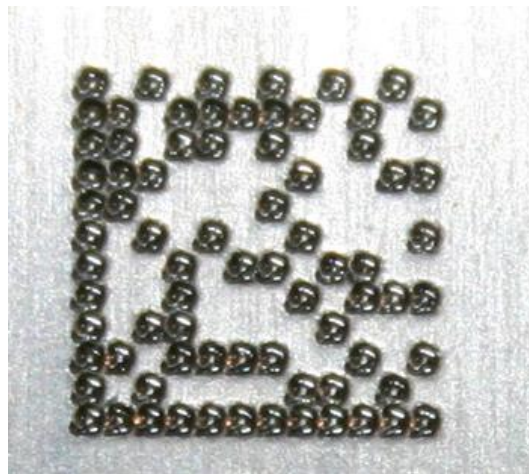
Figure 21: Typical dot peen direct part mark [14].

4. Experiment Three

The outcome of Experiment Two was the hypothesis that shadows are a dominant source of contrast within a symbol image. It was hypothesized that dot peen data matrix symbols utilize the effect of shadows well. The goal of Experiment Three is to test the effect of shadows by replicating the contrast mark geometry of the dot peen data matrix symbol. This geometry will be referred to as Dimple marks for the remaining discussion. The objective of Experiment Three is to evaluate the symbol grade performance of Dimple marks to compare to Bump mark performance. To do so, a casting was created and analyzed using the same basic strategy as in Experiment Two. If symbol grade and specifically Print Growth grades improve, it will demonstrate the ability of Dimple Geometry to control the location of contrast mark through the use of shadows.

The procedure to produce the Dimple mark castings made it necessary to create a new urethane pattern that was the reflection of the original Bump mark pattern. The new urethane pattern was used to create symbol cores that were placed in the same mold assembly as used in Experiment Two. The mold assembly was poured in aluminum to create the Experiment Three casting. A single symbol from the casting is shown in Figure 22. Two of the twelve symbols on the casting were analyzed using an identical vision system and grading strategy as used in the Experiment Two.
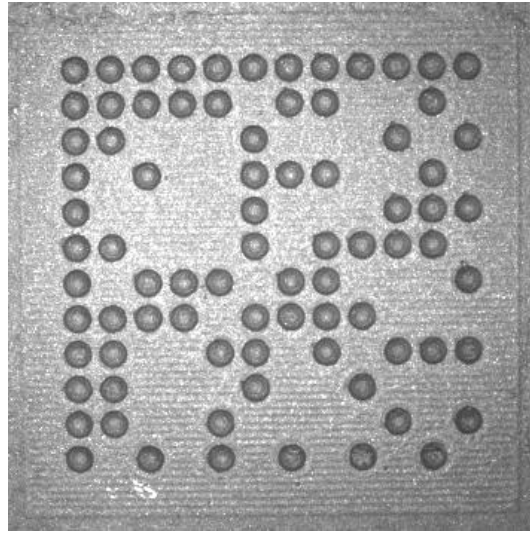
Figure 22: Cast dimple symbol from Experiment Three casting.

4.1.1. Experiment Three Results

The Dimple mark symbol grade results are shown in the Table 10, also shown in the table are the results from the Bump mark symbols from Experiment Two. The results indicate that the Dimple marks outperform the Bump marks in both symbol grade and read rate.

Table 10: Dimple vs. Bump mark symbol grading and read rate results from Experiment Three shown below. All symbol grades on out of a possible 4.000.

Symbol Type	Read Rate	Print Growth Grade	Symbol Contrast Grade	Overall Grade
Dimple	100%	2.50	2.92	2.330
Bump	57%	0.43	1.02	0.233

4.1.2. Experiment Three Conclusion

Experiment Three results indicate that Dimple marks perform superior to Bump marks in read rate and overall symbol grade for Experiment Three. Figure 23 summarizes the grade criterion constraint with Dimple design, which shows that Print Growth is still the primary factor in suppressing overall symbol grade. However, Print Growth is less of a factor than was seen with Bump module geometry.
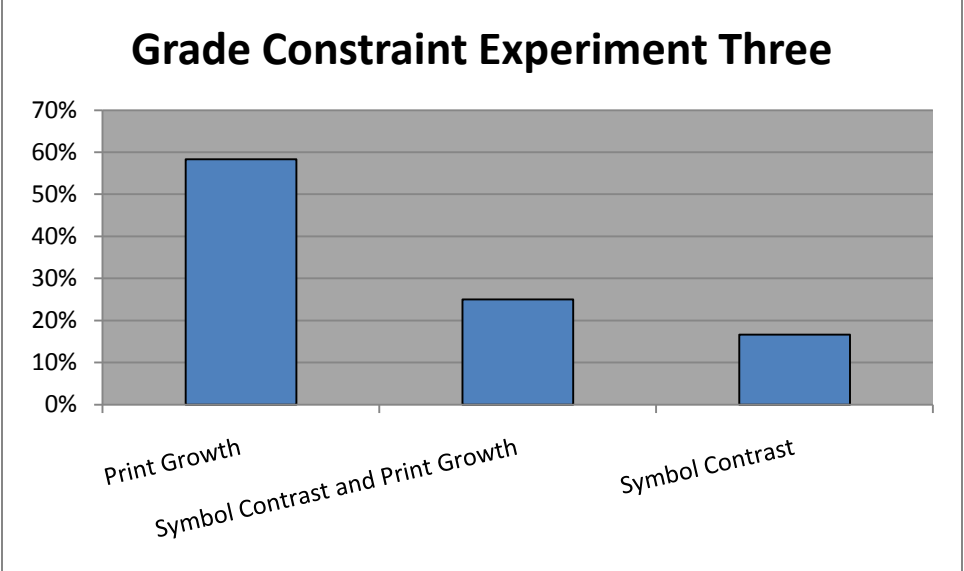
Figure 23: Grade constraint Pareto results for Dimple module design.

The development and control of shadow location are hypothesized to be the primary cause of the measured improvement. The illustration in Figure 24 shows the expected shadow locations for Bump marks, where the shadows locations are opposite direction of the light path.
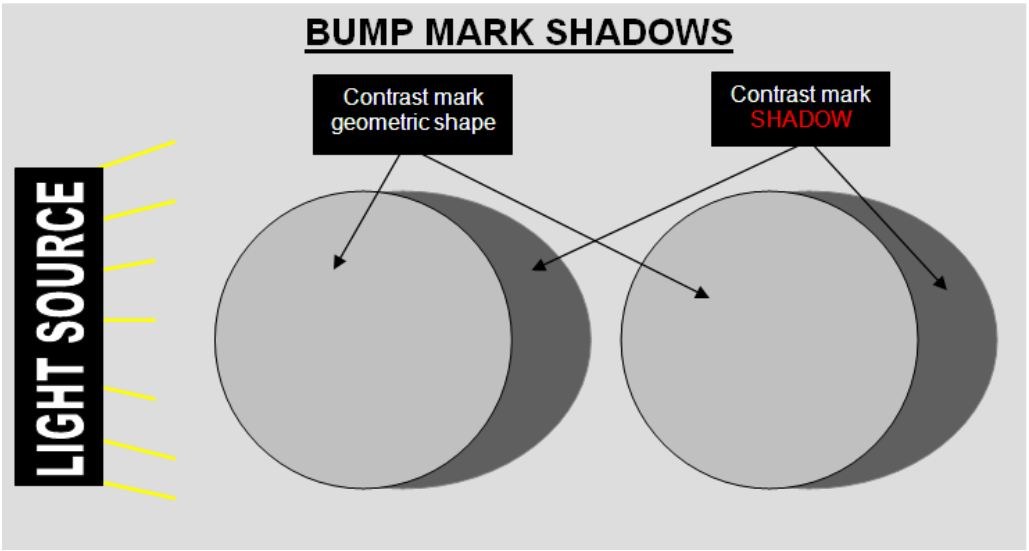
Figure 24: Print Growth calculation.

The performance of Print Growth was much improved with the Dimple marks, which pointed to the importance of shadow placement within module boundaries as a key factor for improved symbol performance. Figure 25 shows the observed shadow location for Dimple mark geometry. The shadow location is confined to inside the boundaries of the contrast mark geometric shape formed by the dimple.
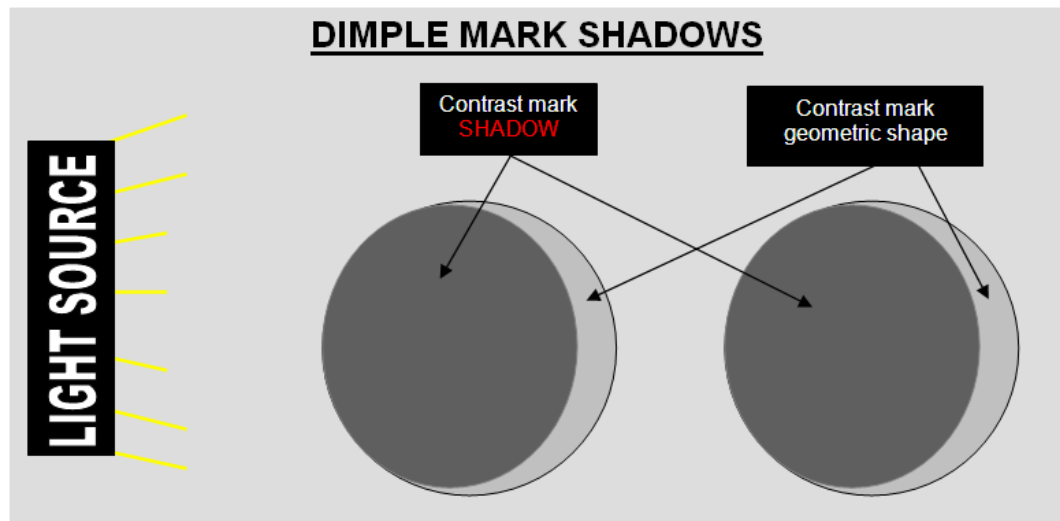
Figure 25: Dot peen shadow width calculation.

The experimental results indicated Print Growth was improved for Dimple marks. However, the specific cause of this improvement was not identified in the grading data. It was assumed the improvement is due to the precise placement of contrast, controlled by the formation of shadows within module boundaries. To verify this assumption, a measurement system with the ability to analyze contrast marks at the module level was needed. The system needs to identify contrast marks using the same method as the imaging system used with Experiment Two and Three to decode and grade the cast samples. Also, the system needs to provide output data regarding the placement and size of contrast marks.

5. Experiment Four

The results of Experiment Three indicate Dimple marks may perform better than Bump contrast marks. Shadow placement is assumed to be responsible for this increase; however there is no data to support this claim. A measurement system was created to capture and analyze image shadows at a range of light angles to provide data on shadow location and size. The images of Bump and Dimple cast symbols were used to calculate:

- The centroid of Bump and Dimple shadows to determine the distance from mark to shadow center.

- Modified Print Growth value, used to approximate Print Growth between two adjacent modules

Using the system and data, a determination can be made as to why Dimple marks outperform Bump marks.

5.1 Experiment Four Setup and Procedure

To facilitate the analysis, a fixture to locate a symbol, camera and light source was necessary so specific light angles could be set and accurate image replications could be obtained. The fixture design is shown in Figure 26. Also, a method to measure the two previously identified critical symbol grade metrics; Print Growth and Symbol Contrast, was necessary for the experimentation. The development of these system aspects are discussed in the following.
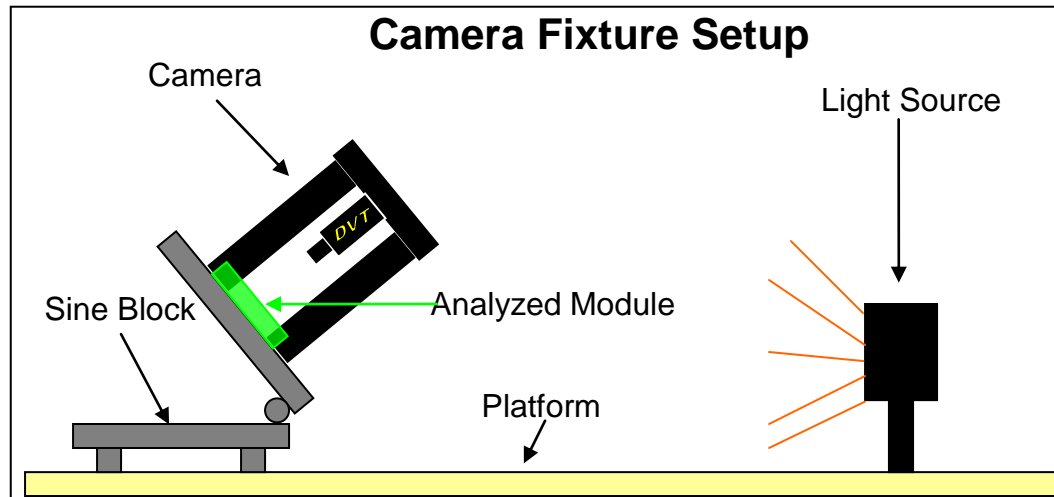
Figure 26: Image acquisition setup for analyzing test modules, which provided repeatable measurements.

Camera Fixture

To evaluate Print Growth for the experimentation, control of incident light angle and module location relative to camera line of sight was critical. A fixture for light angle and contrast mark location relative to the camera was created to control these factors. The fixture consisted of three components: a sine block, rigid platform, and light source. A sine block can be adjusted to specific angles relative to horizontal, which was necessary to control incident light angle. The range of light angle values used for the experimentation was 5, 30, 45, and 60 degrees. The light source and sine block were both attached to a plywood cutout that served as a rigid platform, which allowed the precise image replication.

DVT Camera and Framework Software

To acquire and evaluate images, a DVT Camera Series 600 was used for the experimentation. Once an image is obtained from the camera, it is processed and

analyzed using FrameWork PC software. FrameWork allows users to interface with the DVT camera through a PC and is used to facilitate the measurement of image features using special graphical tools, which identify image features. The tools are referred to as 'SmartSensors' and use variation in pixel intensity within an image to identify contrast features. In the experimentation, contrast features were analyzed for location, size and range of pixel intensity.

Image Analysis Procedure

For image analysis, measuring shadow dimensions and pixel intensity variation within the module space was critical. The SmartSensor utilized for this purpose is referred to as a 'Blob' sensor. Blobs in FrameWork are defined as areas of connected pixels of similar intensity [10]. The Blob sensor searches an image pixel array for adjacent pixels with similar intensities. These pixels are then groups together into a composite contrast mark. Figure 27 shows a set of 'Blobs' identified by FrameWork in the left image, while the original image with the mark shadows is shown to the right. The Blob sensor output data used for analysis was the following: Blob center point and Blob bounding box horizontal width; and minimum and maximum pixel intensity in the search area.
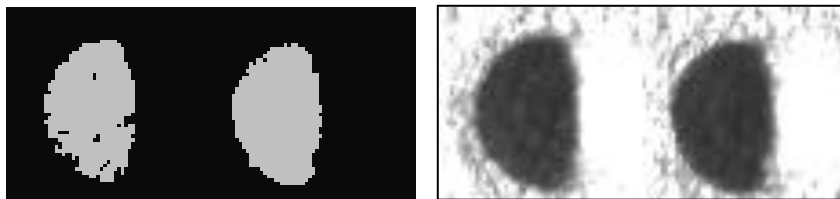
Figure 27: Blob SmartSenors identification results for imaged contrast marks.

Framework data is used to approximate ISO 16022 Print Growth calculation using a modified calculation, referred to as Print Growth$_m$. ISO 16022 requires the execution of the symbol Reference Decode Algorithm to calculate Print Growth. As part of the Reference Decode Algorithm, the average of all module column and row widths is determined as the symbol X value. Using the X value, the deviation for all rows and columns in a symbol are averaged to calculate the Print Growth value. Print Growth considers deviation all sources including material defects, process anomalies in the geometric shape of the symbol, in addition to shadows. The focus of this research was to understand deviation due to shadow formation alone, therefore Print Growth$_m$ was developed to measure mark shadows at the module level.

Print Growth$_m$ measures shadow formation at the individual module level to prevent inadvertent influence of other sources of variation not related to shadow formation. The process used to calculate Print Growth$_m$ is shown in Figure 28. To calculate Print Growth$_m$, the identification of contrast mark center points and widths is obtained from the FrameWork output data. Print Growth$_m$ values range from 0 to 100 percent, with the ideal value being 100 percent, indicating complete fill on the module boundary by the contrast mark.
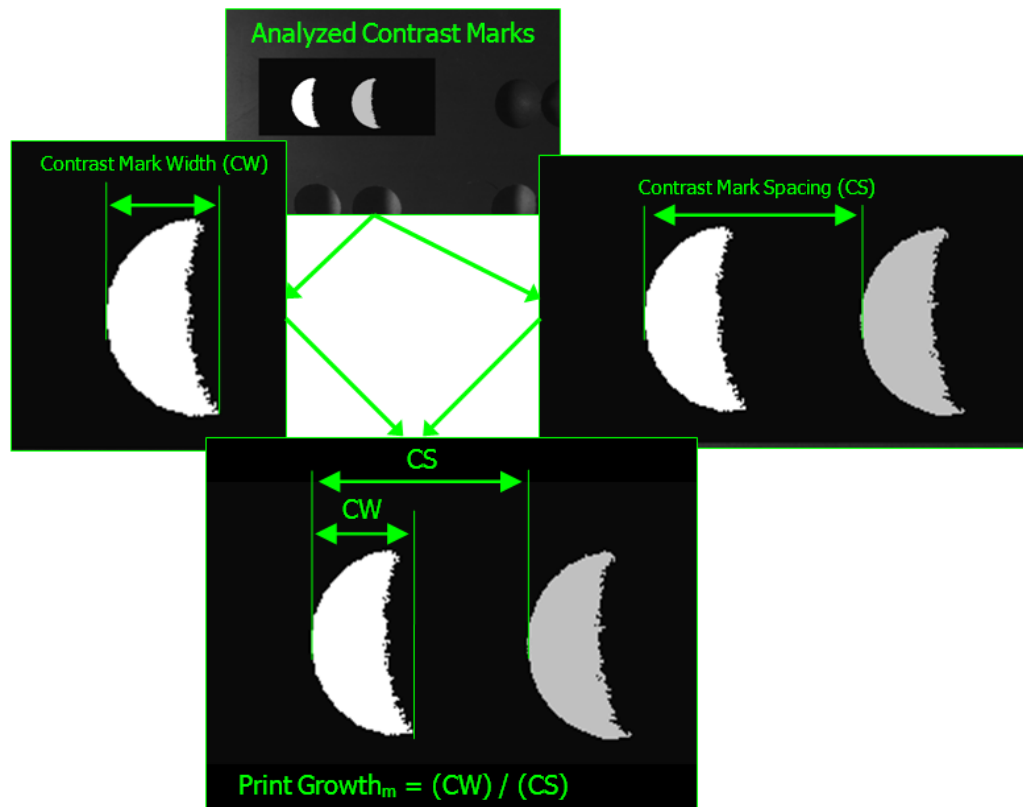
Figure 28: Print Growth$_m$ is the ability of a contrast mark to appropriately fill a module boundary. The width of the left most contrast mark and the distance between the two contrast marks are used to approximate ISO 16022 Print Growth.

In addition to calculating Print Growth$_m$, Symbol Contrast was calculated, which is defined as the difference between the lightest and darkest pixel intensity of all inspected pixels. This information was also generated by FrameWork software. Figure 29 shows the inspection area which is searched to find the lightest and darkest pixel intensities used for calculating Symbol Contrast.
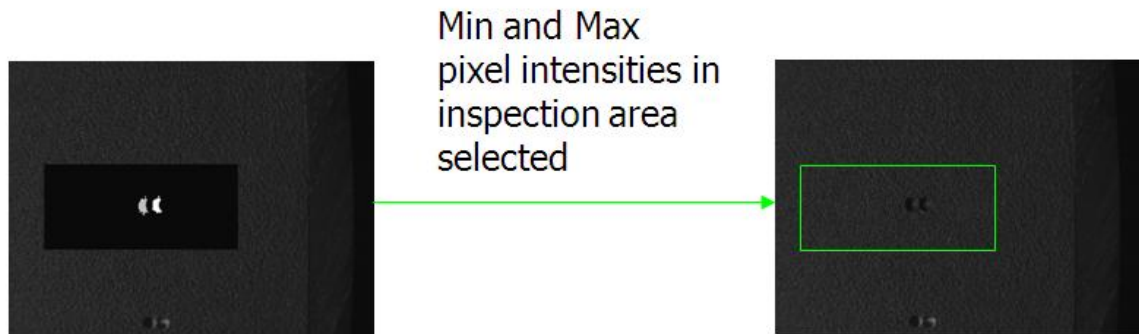
Figure 29: Area in green box shows the inspection area, pixels in this area are evaluated for Symbol Contrast.

To determine the centroid of the mark shadows, an image of a representative sample set of both mark types was analyzed with 30 degree lighting angle for both sets. The analysis included establishing a grid pattern for the sample that is approximately equivalent to module spacing established during the execution of the reference decode algorithm as defined in ISO 16022. In lieu of executing the reference decode algorithm, this grid was created through the use of visual inspection to identify features in the image that correspond to those identified during the algorithm execution.

Once the grid was in place, a bounding box was placed around the shadow, again by means of visual inspection, to establish the shadow boundary approximate location. To compensate for the irregular shape of the mark shadows, the bounding box space was binarized to identify regions within the box that were not shadowed. The binarization process was executed by means of visual inspection of each region element defined as a square region of 0.1 modules.

Once the binarized space contained by the shadow bounding box was identified, the centroid of a polygon that approximated the shadow shape was calculated. Also, the approximate center point location of the geometric feature that created the shadow was identified, which was assumed to be centered in its respective module space. The two coordinate values for the shadow centroid and the geometric feature center point were used to calculate the shadow center distance value. This value represents the shadow offset distance created by the geometric feature.

The analysis procedure for Print Growth$_m$ involved the measurement of single module pairs from castings of each type, Bump and Dimple. Each module pair was imaged at four light angles. At each light angle the module pair was imaged five times and analyzed for Print Growth$_m$ and Symbol Contrast. All five Print Growth$_m$ and Symbol Contrast values were averaged for the final image result. The cast symbols used for the analysis are shown in Figure 30.

Dimple Contrast Marks   Bump Contrast Marks

Figure 30: Cast specimens with Dimple and Bump mark geometry analyzed using DVT camera for Print Growth$_m$ and Symbol Contrast to further verify previous grading results.

5.2. Experiment Four Results

Bump and Dimple symbols were both analyzed to determine if a difference in shadow placement was observed. Figure 31 shows the cast shadows at a 30 degree light angle, which were used for centroid analysis.

Bump Marks   Dimple Marks
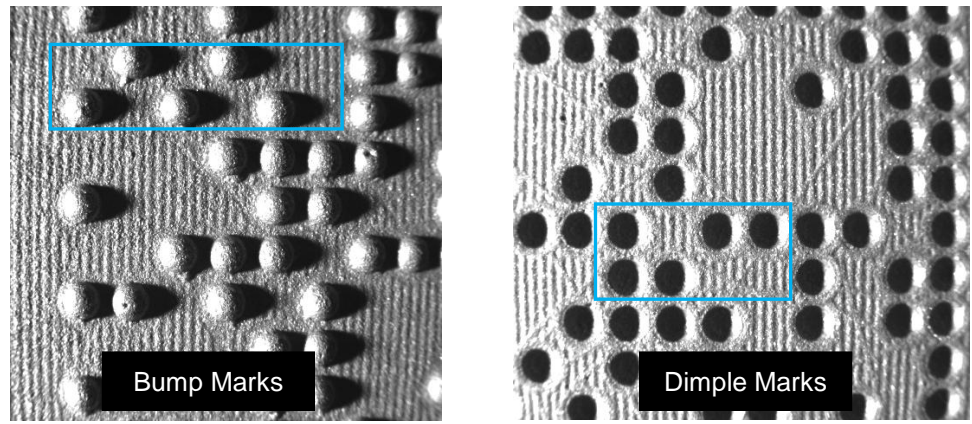
Figure 31: Bump vs. Dimple shadows at 30 degree light angle, the centroid inspection space identified by the blue box.

A sample section from each mark type was used in the analysis shown in Figure 32. The analysis includes the calculation of the shadow centroid to compare to the identified geometric shape center point.
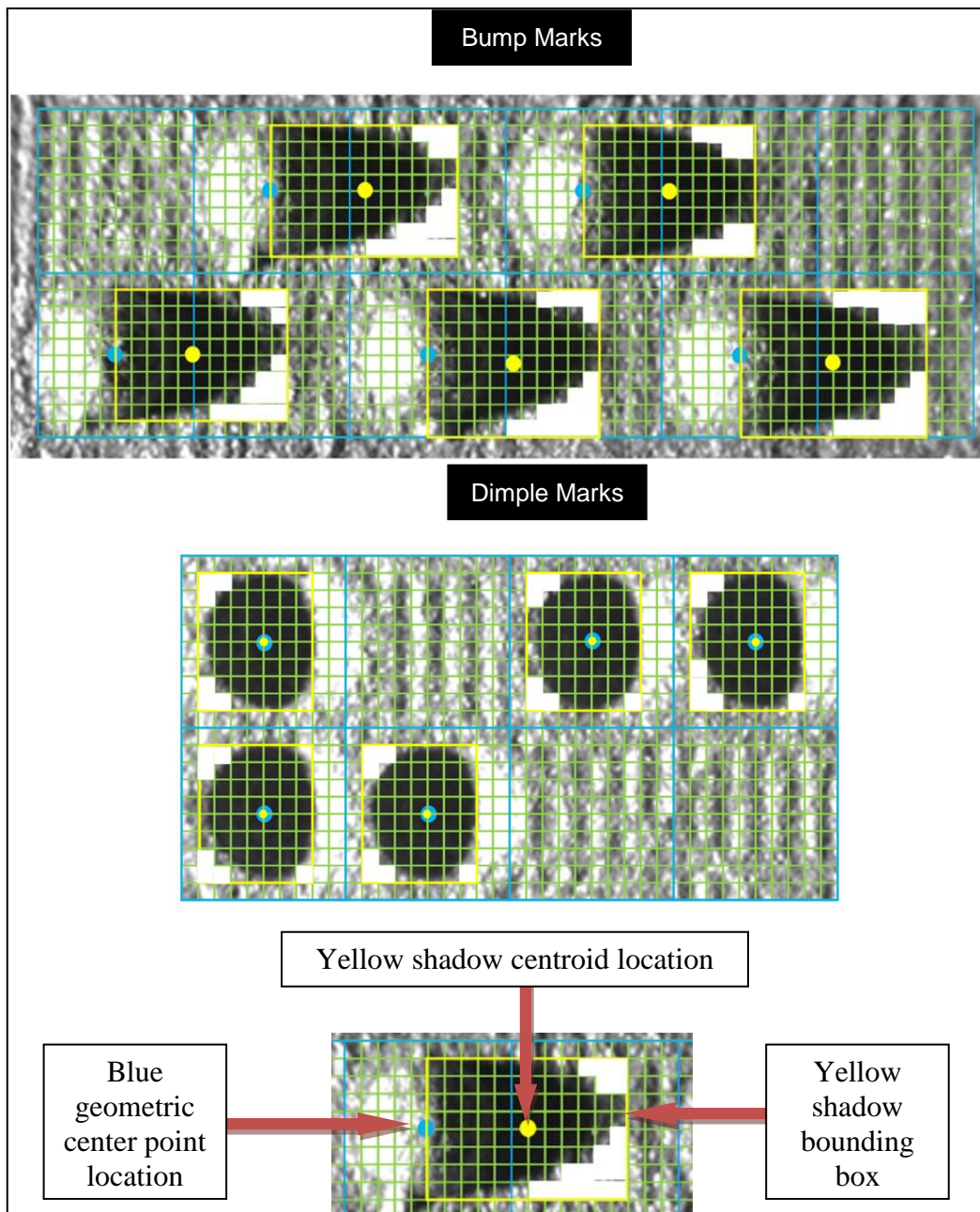
Figure 32: Centroid measurement for both Bump and Dimple marks. The centroid location is depicted by the yellow circle, while the geometric mark center point is shown by the blue circle.

The results of the centroid analysis are shown in Table 11 and 12. These results indicate that the shadow center point to be larger for Bump modules than for Dimple modules, with a difference of 0.5 module to zero modules for Bump marks and Dimple marks, respectively.

Table 11: Results on the centroid analysis for Bump marks. The results indicate the average distance from centroid the center point to be 0.5 modules.

	Centroid		Center Point		
Mark	X	Y	X	Y	Distance (0.1 modules)
1	5	4	0	4	5
2	5	4	0	4	5
3	5	5	0	5	5
4	5	4	0	4	5
5	5	5	0	5	5

Table 12: Results for the centroid analysis for Dimple marks. The results indicate the average distance from centroid to center point to be zero modules.

	Centroid		Center Point		
Mark	X	Y	X	Y	Distance (0.1 modules)
1	4	4	4	4	0
2	4	4	4	4	0
3	4	4	4	4	0
4	4	4	4	4	0
5	4	4	4	4	0

The issue with shadow containment is highlighted with the observed interference of adjacent modules seen in Figure 33. In the image, the FrameWork inspection area is shown with the identified blobs in grey against the black background. At 5 degree light angle, the Bump marks symbol becomes unreadable due to the pervasive shadow interference. The inspected module pair is highlighted in the red box, while the adjacent module is circled in blue showing the interference condition. The Dimple mark module

pair at 5 degree light angle is shown highlighted in the green box with much improved

contrast mark definition and no interference.
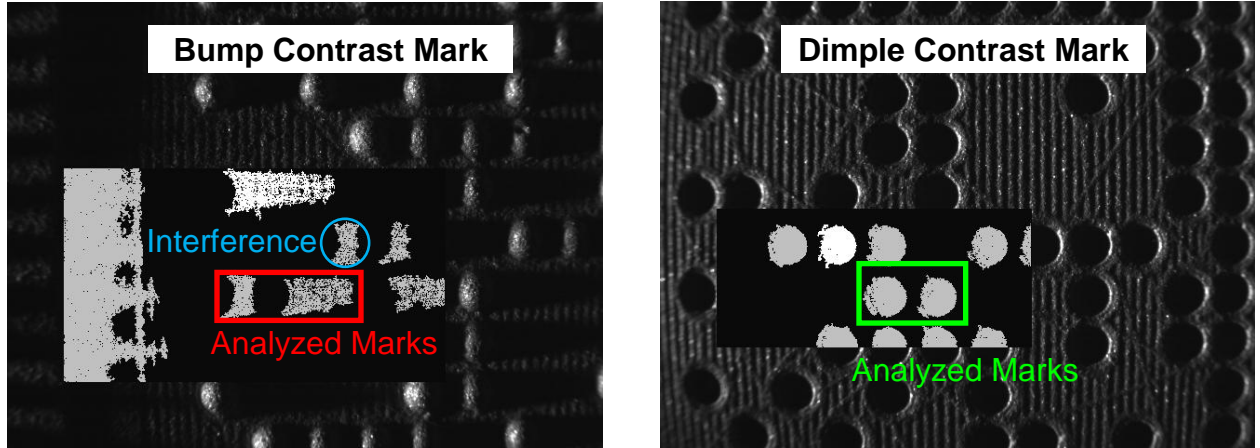
Figure 33: Five degree light angle contrast mark performance comparison.

The analysis of Print Growth$_m$ and Symbol Contrast was executed and results tabulated in

Table 13. Two observations can be made from the results:

- At 5 degree Bump marks were not readable

- The range for Bump Print Growth$_m$ was greater than Dimple due to nature of

  shadow formation at various light angles

Table 13: Results of Dimple and Bump mark geometry for Print Growth$_m$ and Symbol Contrast.

Light Angle (Degrees)	Print Growth$_m$	Symbol Contrast
Bump Mark		
5	-	-
30	80%	93%
45	40%	90%
60	43%	95%
Dimple Mark		
5	78%	96%
30	62%	88%
45	59%	83%
60	59%	93%

At 5 degree light angle, the elongation of shadows for Bump marks was pervasive to the point interference prevents decoding the symbol as illustrated in Figure 33. In this case, the shadow exceeds the module limits considerable preventing the reference decode algorithm from identifying individual contrast marks in the symbol.

The results also indicate that Dimple mark Print Growth$_m$ was lower than Bump mark Print Growth$_m$, for light angle 5 and 30, while it was higher at 45 and 60 degree light angles.

The total range of Print Growth$_m$ for Bump mark shadows was 37 percent, while it was 19 percent for Dimple mark shadows. The wider Print Growth$_m$ range indicates light angle is more critical to Bump marks than Dimple marks and that Bump marks shadows are more susceptible to variation due to light than Dimple mark shadows. At a 30 light angle Bump mark Print Growth$_m$ is greater than Dimple mark Print Growth$_m$. In this instance, the greater value is due to correction caused by averaging the two Print Growth$_m$ values for the pair of shadows created by the Bump marks. In reality there is a large difference between the two shadow sizes that is illustrated by calculating the difference in shadow size. At 30 degree light angle the difference in shadow size was 31 percent for Bump marks. At 30 degree light angle, however, the difference in shadow size for Dimple marks was calculated at 6.5 percent. This is also a source of variation that correlates to poor performance of Bump mark.

Given the positive results of the Dimple mark geometry, further analysis was needed to understand the formation of shadows at various lighting angles. It was observed shadow size changed depending on the light angle. It was inferred changes in shadow shape due to changes in light angle could potentially affect Print Growth$_m$. To estimate expected size of shadows, a model was created to provide a basis for symbol design in future applications.

6. Shadow Width Model

The conclusions of the Experiment Two pointed to Print Growth as the primary grade factor limiting symbol decode performance of Bump mark geometry. While Experiment Three indicated that Dimple marks could improve shadow location control compared to Bump marks. To approximate expected symbol grade performance, a model was needed to determine the size and placement of contrast marks using Dimple mark design. Model information could be utilized as an approximation of Print Growth performance.

Figure 34 gives the side and top view of the Dimple mark geometry and shadow. The views depict the assumptions of the model. The assumptions include a spherical body intersected by the x-y plane. The top view shows the shadow of a Dimple mark and the incident light orientation. The top view is important because it represents the view of an imaging device. It was observed in Experiment Four that shadow-width distance varies from point A to B dependent on light angle. The model objective is to predict shadow width distance at various light angles for the Dimple mark geometry.

Model Side View

y

Dimple mark
geometry

z

Top View

y

Shadow boundary

A Width? B

Light

x
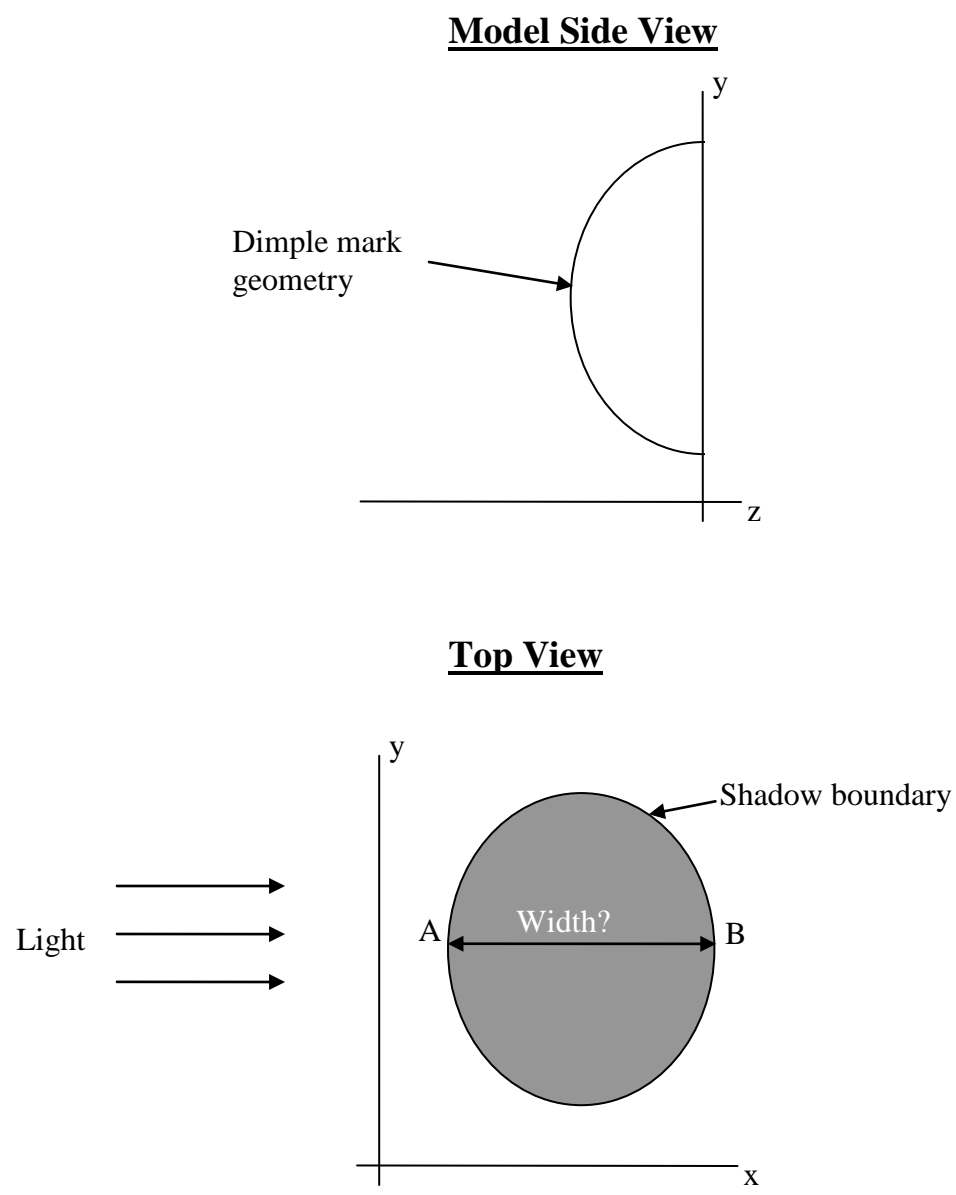
Figure 34: Dimple mark geometry side and top view showing the orientation of the light relative to the shadow and geometry.

6.1. Shadow Model Overview

The location of the image sensor, light source, and casting surface possessing the Dimple

mark geometry are important to the shadow model construction. The orientation of the

line of sight from image sensor to casting surface is considered orthogonal. The Dimple

mark geometry is a hemisphere with negative z coordinate values. The incident light is approximated using a plane intersecting x-y plane, which represents the castings surface.

6.2. Shadow Model Development

A shadow function was developed to approximate the Dimple mark geometry shadow boundary. The shadow function is an algebraic description of all points that lie within the region contained by the intersection of a hemisphere and the plane of light. This region is an approximation of the shadow when viewed in the negative z direction.

It was necessary to first determine the function describing the incident plane of light emanating from the light source. To determine the light plane equation, the angular components of each axis coordinate are calculated. The variables *a*, *b*, and *c* represent the coefficients of a plane equation normal vector, $\vec{n}$ and are dependent on the light plane orientation as shown in Figure 35.

In the model, the light plane equation intersects the hemisphere at a point coincident with the x axis. The incident light angle relative to the x-y plane is given by θ. The normal vector component, *b*, is set to zero for the two dimensional vector set in x-z space. The components of the normal vector are given in the following.

Normal vector (light plane): $\vec{n} = \langle a, b, c \rangle = \langle -\cos(90 - \theta), \quad 0, \quad \sin(90 - \theta) \rangle$
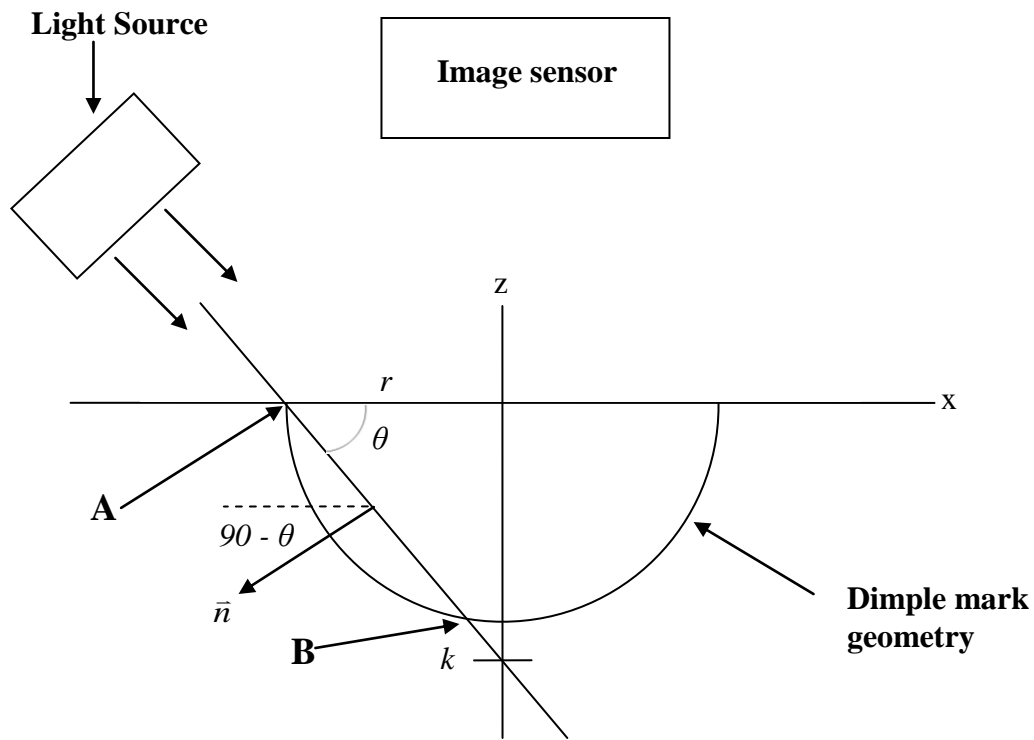
Figure 35: Geometric model of marking and light interaction.

The plane equation is solved for values of z to give the function, *f(x, y)*, shown below:

$$ax + by + cz = ck$$

$$ax + (0)y + cz = ck$$

$$f(x, y) = z = k - \frac{ax}{c}$$

The hemisphere is given by the following equation, where *r* is the hemisphere radius:

$$r^2 = x^2 + y^2 + z^2$$

The distance from the origin to the light plane intersection along the z axis is *k*, shown in the function below:

$$k = r\tan(\theta)$$

To determine the function that describes the shadow region, the z equation from the plane equation is substituted into the hemisphere equation. Figure 36 is an illustration of relative location of a shadow region when $0° < \theta < 90°$.
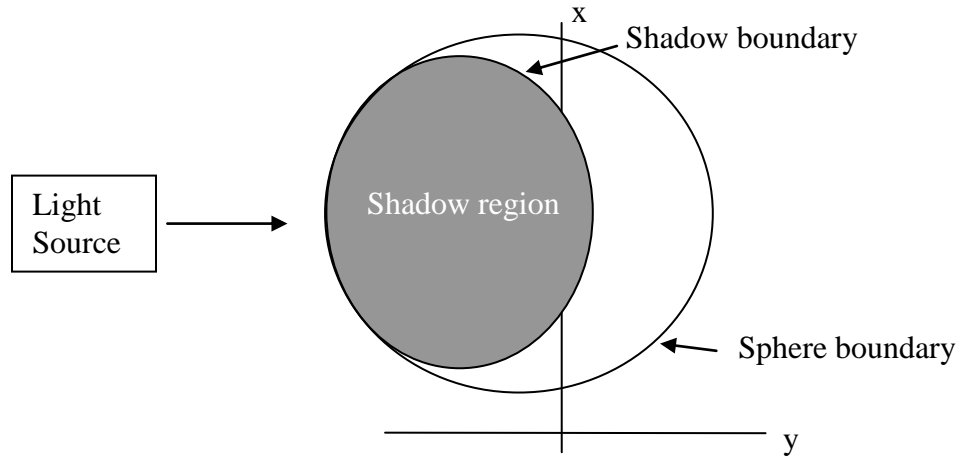
Figure 36: Shadow boundary inside hemisphere.

After substituting the z coordinate function into the sphere equation, the following gives the equation for shadow region:

$$f = x^2 + y^2 + (k - (\tfrac{a}{c})x)^2 - r^2$$

The bounds of the shadow region are used to determine the width of the shadow along the *x* and *y* axis. The bounds in each direction are calculated separately. The shadow boundary along the *x* axis is found by setting *y* equal to zero and solving *f* for *x*. The quadratic function is solved for two roots representing each half of the boundary shown below:

$$\alpha_1 = \frac{ack + c\sqrt{r^2 a^2 - c^2 k^2 + r^2 c^2}}{a^2 + c^2}$$

$$\alpha_2 = -\alpha_1$$

Using a similar method the bounds of the shadow region along the *y* axis are found by setting *x* to zero and solving *f* for *y*:

$$\beta_1 = \sqrt{r^2 - k^2}$$

$$\beta_2 = -\beta_1$$

Once the model shadow boundaries were calculated, values for *θ* and *r* were used to create a set of solutions. The radius, *r*, is set equal to ten, which is without units so as to allow it to be extended into any system of units. A range of values for *θ* was solved between zero and 60 degrees. After the value for a, c, and k are calculated, the results are in Table 14.

Table 14: X and Y shadow widths at various light angles based on model shadow boundaries. The model is without units.

Angle(*θ*)	X	Y
0	20.0	20.0
30	15.0	17.3
45	10.0	14.1
60	5.0	10.0

The model results indicate that as the light angle approaches zero, the shadow width increases. In general, larger shadow widths will result in greater module fill and improve Print Growth. The conclusion is that as light angles approach zero, the result will be improved Print Growth values. Using this results and additional experiment was planned to further analyze shadow creation at the module level. It was identified that spacing between contrast marks could be a potential factor that could affect symbol grade performance and read rate, but may be a limitation of the process producing the symbol. In addition to spacing, mark diameter and surface roughness could play roles in symbol performance. These factors were considered in the following experiment.

7. Experiment Five

The symbol grading results of Experiment Four pointed to the superior performance of Dimple mark geometry due to module placement and size. To further explore the performance of Dimple mark geometry, a model was created to predict shadow width given specific light angles. The model indicates light angles closer to horizontal give larger shadow width, which equate to larger contrast marks, improved Print Growth grades, and symbol performance. Experiment Five evaluates light angle as a factor due to the connection between image contrast marks and module shadows. An empirical result for shadow width was needed to determine the performance of the shadow model. Also, symbol design will depend on results relating to the effect of surface roughness, module spacing and diameter, which the shadow model does not consider. The affect of these factors on Print Growth and Symbol Contrast are also unknown.

To improve understanding of these factors, experimentation was completed using test modules to approximate the performance of symbols from cast surfaces.   The test modules were fabricated using a method to control surface roughness values. The goal of experimentation was to evaluate Print Growth$_m$ and Symbol Contrast at the module level, while controlling surface roughness and module diameter and spacing. In practice, personnel responsible for designing a process to produce sand cores to create cast data matrix symbols will experience a tradeoff between symbol performance and process capability, due to limitations in the precision in which geometric features can be produced. This will affect the size of module diameters and the spacing between modules. The affect of increasing module diameter on the reference decode algorithm

result will be a change in module size calculated during execution. For module spacing, the affect on reference decode algorithm result will relate to the degree to which the shadows produced by the geometric features fill the module space and the module size calculated during execution. This affect is relevant to symbol performance and relate directly to Print Growth grading as shown in Figure 37.
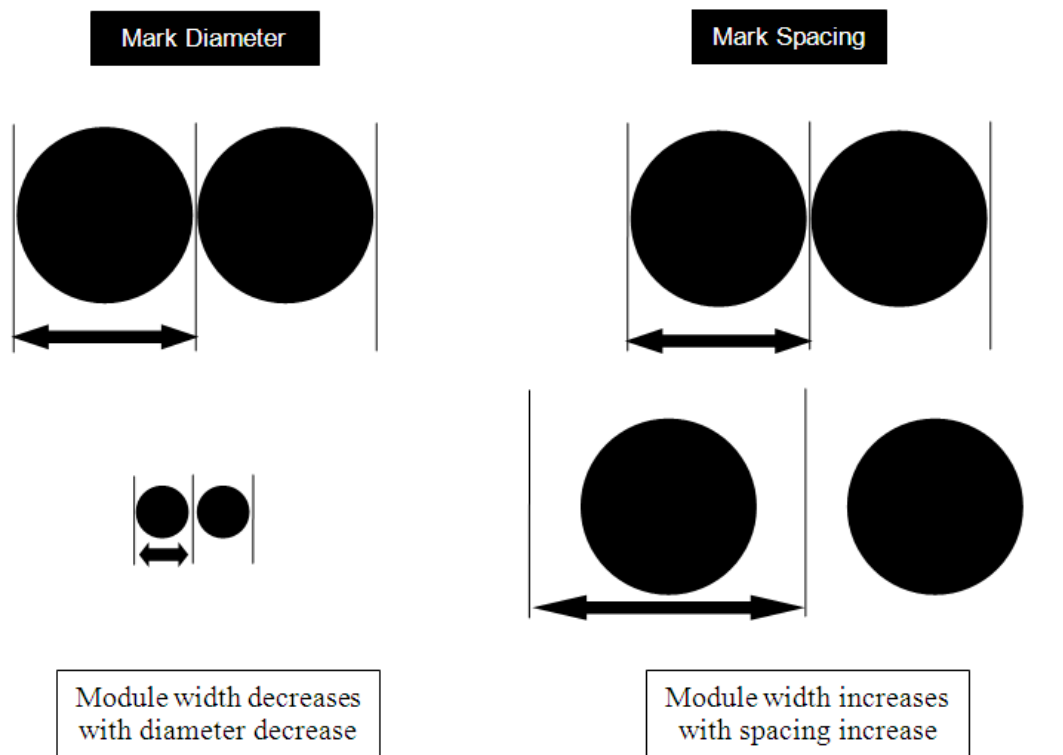
Figure 37: Affect of changes in module diameter and spacing on module width.

7.1 Experiment Five Setup and Procedure

Test Module Development

Surface roughness was a key factor of the experimentation. To control surface roughness, test modules were created, shown in Figure 38. Four levels of surface roughness were evaluated to allow the results to be applicable to an array of casting surface finishes. A

mechanism for surface roughness control was devised to allow the evaluation of Print Growth$_m$ and Symbol contrast for different levels of surface roughness.

In addition to surface roughness, mark geometry was critical. To measure Print Growth$_m$ two adjacent modules must be analyzed, therefore test modules were created in pairs. It was hypothesized that closer spacing would yield improved results, but the practicality of closely spaced modules may not be feasible in all cast symbol production. Also, it was hypothesized that module diameter would affect evaluation results. To determine the effect of spacing and diameter, various levels were evaluated for Print Growth$_m$ and Symbol Contrast.

To fabricate the test modules, grey urethane was poured into pattern cavities. The grey urethane was selected due to its physical approximation of a cast surfaces. The surface roughness control method consisted of using a sand paper lined pattern to create the test module specimens. The four levels were smooth (no sandpaper), 120, 80, and 40 grit sand paper. After pouring the urethane, each piece was drilled with a ball end mill to create the test modules. The module diameters were as follows: 0.0625, 0.125, and 0.25 inch. Each module set was spaced at 0 percent, 25 percent, and 50 percent of the respective module diameter.

After the prototypes were produced, the surface roughness was evaluated using GAR Electroforming C-9 comparator plate with known RMS surface roughness values as a reference for inspectors.
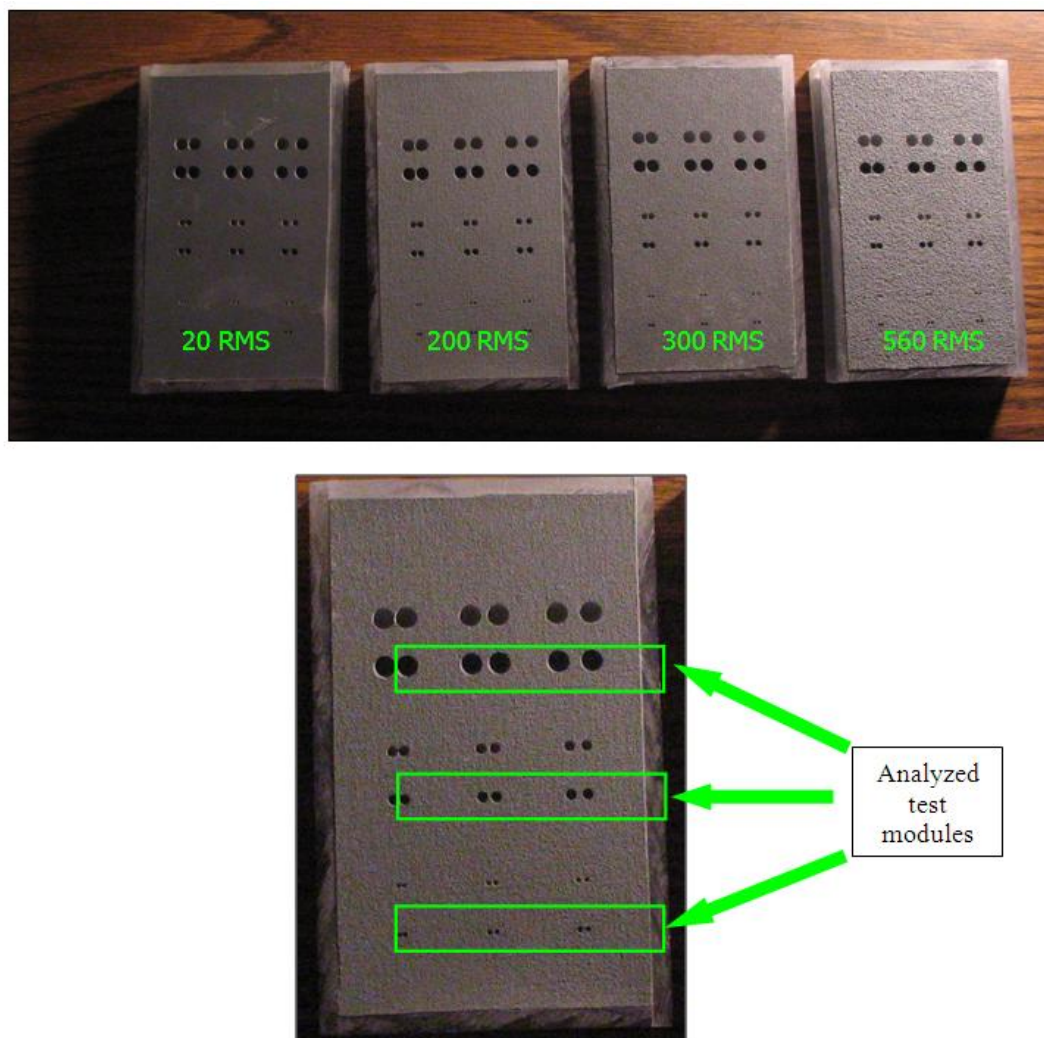
Figure 38: Test module specimens used to evaluate performance of Dimple contrast marks at four levels of surface roughness. The module sets contained in the green boxes were those that were evaluated for the experimentation for each surface roughness level.

Six inspectors from a metal castings foundry were presented with the test module specimens and asked to grade each using the comparator plate as a reference; results of all inspections are shown in the Appendix.

Using the mode value of all inspection results for each specimen, it was estimated the test module surface roughness levels were 20, 200, 300, and 560. The image acquisition and analysis was the same as that used in Experiment Four to determine Print Growth$_m$ and Symbol Contrast. Once the analysis was complete, the data was used to create the experiment results.

7.2. Experiment Five Results

The planned procedure was executed and results were generated. The goal of the experimentation was to evaluate the performance of the shadow model and determine effect of differing levels of incident light angle, surface roughness, module spacing and module diameter on Print Growth$_m$ and Symbol Contrast. It was assumed, in practice, surface roughness, module spacing and diameter will be determined by estimating a casting process capability, rather than adjusting the process to a specific value. However, light angle would be an easily adjusted process setting and was used to determine an optimum level.

Contrast Mark Diameter

The test module diameter results for Print Growth$_m$ and Symbol Contrast are shown in Figure 39. The average and standard deviation for Print Growth$_m$ and Symbol Contrast were calculated by using all results of module images.
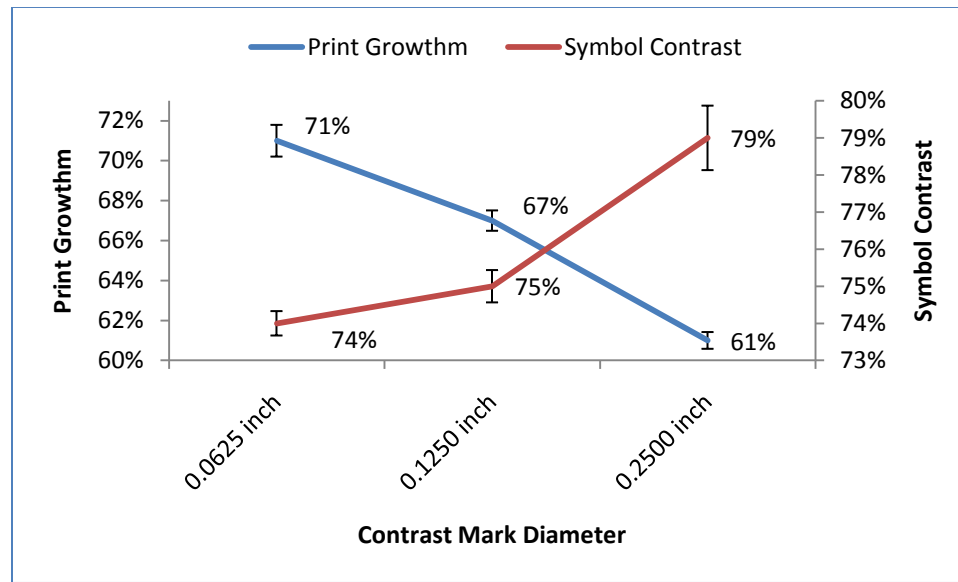
Figure 39: Test module Print Growth$_m$ and Symbol Contrast results for contrast mark diameter. Error bars indicate magnitude of standard deviation for each diameter.

The results suggest the following trend as mark diameter is varied: Smaller mark diameters yield higher Print Growth$_m$ average and standard deviation, while larger marks have the lower Print Growth$_m$ average and standard deviation. Furthermore, as mark diameter is varied, the reverse trend is observed for Symbol Contrast.

Contrast Mark Spacing

Contrast mark spacing was an evaluated factor; results are shown in Figure 40.
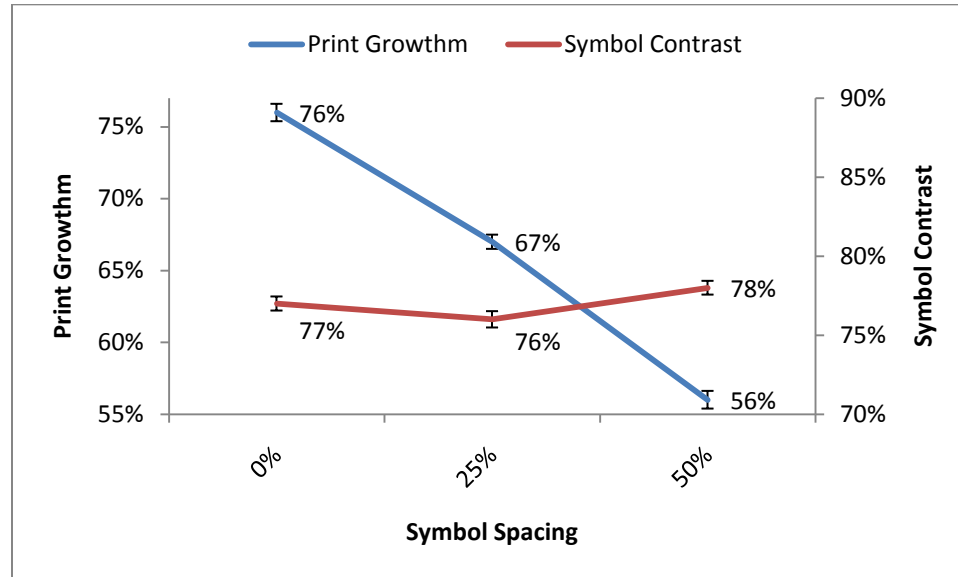
Figure 40: Test module Print Growth$_m$ and Symbol Contrast results for contrast mark spacing.

Symbol Contrast did not demonstrate a strong correlation to contrast mark spacing. However, Print Growth$_m$ was shown to be affected by spacing. The results indicate that as contrast marks are spaced further apart, Print Growth$_m$ decreases.

Surface Roughness

The results of each surface roughness values are show in Figure 41.
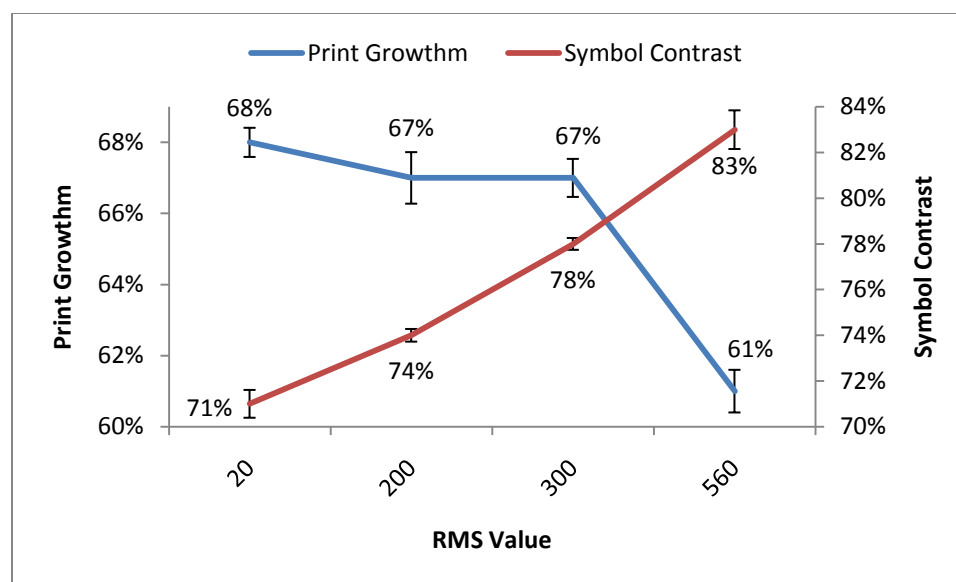
Figure 41: Test module Print Growth$_m$ and Symbol Contrast results by surface roughness.

The results indicate that Print Growth$_m$ remained consistent for each surface roughness value, but a significant decline was observed at 560 RMS. Also, the results indicate that as surface roughness increases, Symbol Contrast also increases.

Light Angle

Light angle is considered a setting of the image acquisition system. Therefore, various levels of lighting angle were considered a part of the experimentation to assist in determining an ideal lighting level. Table 15 presents the results of the one factor ANOVA for Print Growth$_m$ and Symbol Contrast, which finds the null hypothesis is rejected. Rejecting the null hypothesis indicates the affect of varied light angle on Print Growth$_m$ and Symbol Contrast values is substantiated.

Table 15: The table contains a one factor ANOVA table for Print Growth$_m$ and Symbol Contrast, which shows the null hypothesis is rejected for lighting angle. Critical $F_{1-\alpha} = 2.60$ where $\alpha = 0.05$, [13].

Source of Variation (Print Growth$_m$)	Sum of squares	Degrees of freedom	Mean square	F
Between Treatments	3.01	3	1.51	45.50*
Within Treatments	23.71	716	0.03	
Total	**26.72**	**719**		

Source of Variation (Symbol Contrast)	Sum of squares	Degrees of freedom	Mean square	F
Between Treatments	63.52	3	31.76	213.74*
Within Treatments	106.40	716	0.15	
Total	**169.91**	**719**		

The results for average Print Growth$_m$ and Symbol Contrast for the light angle are shown in Table 16.

Table 16: Experimentation results of light angle factor for Print Growth$_m$ and Symbol Contrast.

Light Angle (degrees)	Print Growth$_m$	Symbol Contrast
5	70%	68%
30	68%	86%
45	58%	82%
60	54%	12%

The results indicate five degree light angle produces the highest Print Growth$_m$ average, while 60 degree light angle produces the lowest Print Growth$_m$ average. Also, that Symbol Contrast is best at a 30 degree light angle.

7.3. Experiment Five Discussion and Conclusions

The objective of the experimentation was to understand the effect of contrast mark diameter and spacing, surface roughness and light angle on Print Growth$_m$ and Symbol Contrast. The following is the interpretation of the results.

The observed trend for Print Growth$_m$ was that as diameter increased, Print Growth$_m$ decreased and Symbol Contrast increased. The standard deviation of each diameter average followed the same trend for both metrics. This can be explained by the relationship between contrast mark diameter and image pixel size. Contrast mark shadows do not fill all adjacent pixels completely, as shown in Figure 42, which gives a theoretical illustration of the contrast mark diameter effect on Print Growth$_m$ average and standard deviation. Error results when a shadow partially fills a pixel and is then selected as part of the contrast mark. The sum of error for smaller diameter contrast marks is greater than that of larger diameter contrast marks due to the relationship of the area the mark fills relative to its boundary length.

The cause of Symbol Contrast trend is due to an alternative influence and is attributed to the amount of ambient light incident inside the mark geometry relative to diameter. Symbol Contrast is the difference in intensity between light and dark pixels. The darkest pixels are typically located in the interior of the mark, the larger the mark diameter, the greater population of dark pixels. Intensity values equal to 100 percent equate to the lightest pixel, these pixels are abundant in module images. Therefore, the driving factor in Symbol Contrast is the low intensity of dark pixels within the image. Dark pixels become more abundant in larger diameter marks, as demonstrated in the Experiment Five data. The trends for both Print Growth$_m$ and Symbol Contrast are inverted, indicating a trade off in mark diameter.

Diameter Caused Error
- Pixels containing fringe of contrast mark cause variation in estimating Print Growth calculations
- Larger contrast marks relative to pixel size have less fringe pixels as a total of all contrast mark pixels
- Fringe % is the total fringe pixels of all contrast mark pixels

- Fringe pixel

- Shadowed pixel

"Small Mark geometry"

Contrast Mark Pixels: 18
Shadowed Pixels: 4
Fringe Pixels: 14
Fringe %:   78%

"Large Mark geometry"

Contrast Mark Pixels: 56
Shadow Pixels: 24
Fringe Pixels: 32
Fringe %:   57%
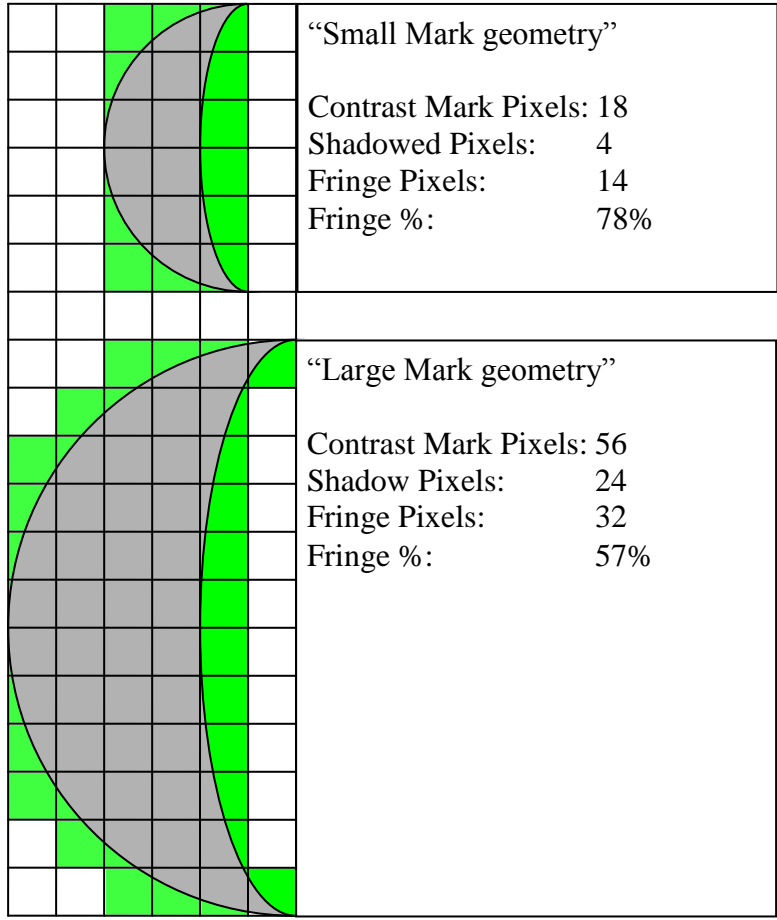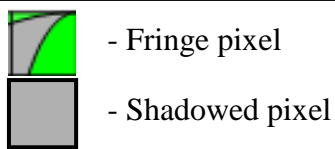
Figure 42: Cause of error in Print Growth$_m$ due to relationship between contrast mark boundary and area.

$$\text{Print Growth}_m = (\text{Contrast Mark Width}) / (\text{Contrast Mark Spacing})$$
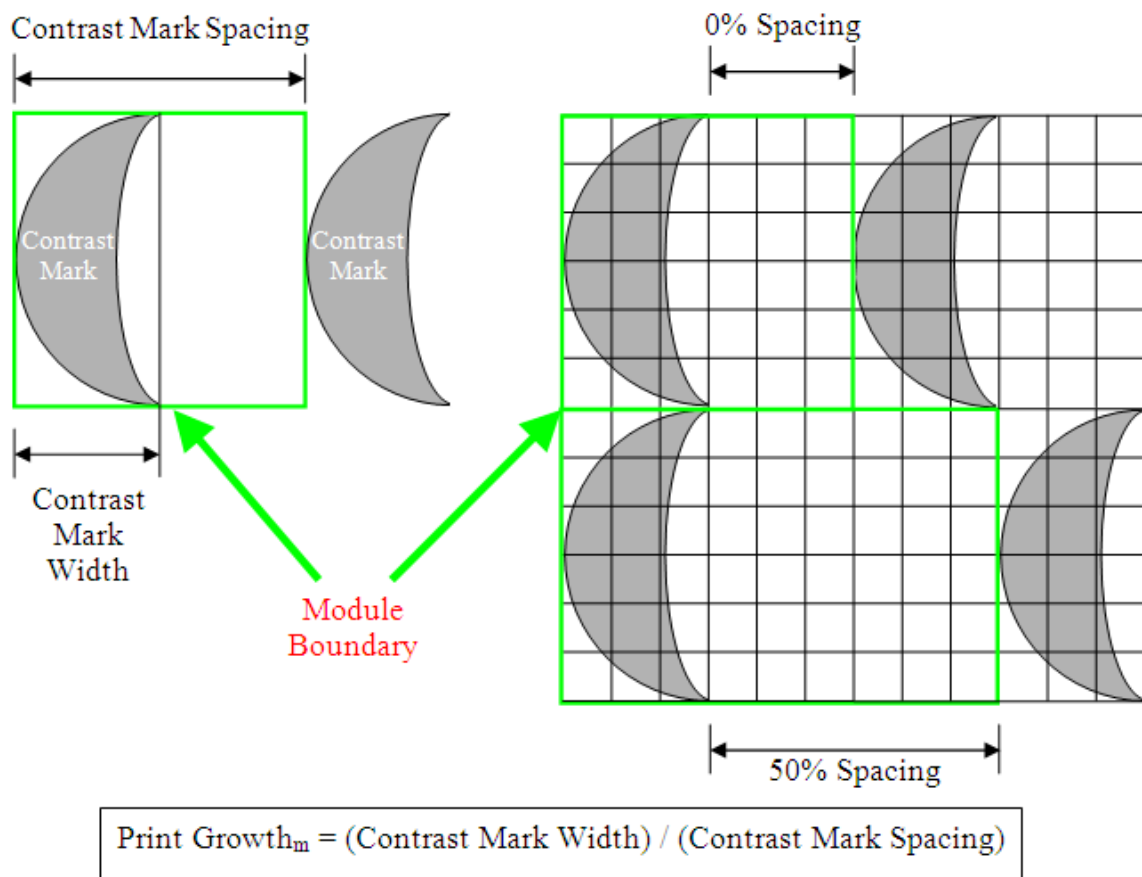
Figure 43: Effect of mark spacing on Print Growth$_m$, as spacing increases, Print Growth$_m$ decreases.
The results of Experiment Five indicate that as spacing increases, so does Print Growth$_m$ while Symbol Contrast appears to be unaffected. The increase in Print Growth$_m$ is likely caused by the decrease in the contrast mark width relative to the module boundaries. If the contrast mark does not grow in area as spacing increases, the contrast mark will effectively fill less of the module boundaries. Filling less of the module space decreases the Print Growth$_m$ value. Figure 43 illustrates this concept.

The observed trend in the results data is that as surface roughness increases, Print Growth$_m$ remains close to level until 560 RMS, while Symbol Contrast shows a clear increase. The trend seen in Symbol Contrast is attributed to additional noise due to the

surface roughness. Surface roughness widens the distribution of pixel intensity values and increases the difference between the darkest and light pixels. The impact of this result is that greater noise within the symbol from surface roughness increases the difficulty in discerning intentional contrast marks from random contrast marks. This condition is to be expected from increased surface roughness, which is in itself, variation. The decrease in Print Growth$_m$ is likely caused by the blob construction process interference from increased surface roughness. The process attempts to group pixels of like intensities into Blobs, which compensates for less than ideal lighting by over sizing contrasted marks. Contrast marks are oversized by including adjacent, non contrasted pixels into the composite blob region.

The light angle is an image system setting, adjustable by the operator. Therefore, the rejection of the null hypothesis for both Print Growth$_m$ and Symbol Contrast indicates that the light angle is a critical factor. The results indicate that the ideal light angle is 30 degrees when considering both Print Growth$_m$ and Symbol Contrast. Figure 44 shows the relationship between the shadow model results, adjusted for contrast mark spacing, and the FrameWork data empirical results of the experimentation. The empirical and model results indicate that the general trend of the model exists in the empirical data generated by the experimentation. The exception is at 60 degree light angle, which is likely due to the blob construction process.
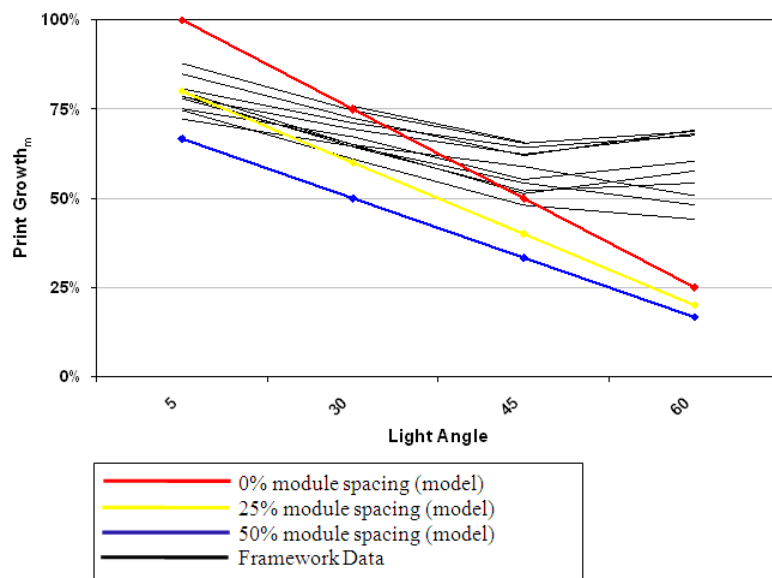
Figure 44: Model results with theoretical effect of spacing versus empirical results of experimentation

8. Symbol Design Application

The applicability of this research to industry was kept as a key consideration of the experimentation as indicated by the use of industry foundry facilities to produce the cast symbols. Also, the test modules were developed to understand the effect of variation in surface roughness values that varies throughout the casting industry. The results of this experimentation provided the basis for a practical recommendation of future cast symbol design applications. The data presented represents the first step in approximating the results to be expected in industry, but as every foundry is different, focused experimentation will be a requirement before the implementation of cast data matrix symbols within any foundry will come to fruition.

The 300 RMS and 560 RMS surface prototype specimens were considered an approximation of aluminum and ferrous casting surfaces, respectively as recommended GAR Electromforming Division Comparator C-9 plate. To facilitate the objective selection of symbol design criteria, a decision heuristic was developed to select the experimental factor criterion for mark diameter and spacing that attempts to optimize symbol design. The decision heuristic used for selection is a shown in below:

[(PGA)/ (PGSD)] – [(SCA)/ (SCSD) X (0.5)]

where

PGA = Print Growth$_m$ Average

PGSD = Print Growth$_m$ Standard Deviation

SCA = Symbol Contrast Average

SCSD = Symbol Contrast Standard Deviation

The heuristic represents the tradeoff between a high average value for each symbol grade component and the level of variation quantified by the symbol grade standard deviation. In the preliminary experimentation results obtained from ECHO Automation, Print Growth was determined to be the limiting grade component that more often affected the final symbol grade. Therefore, Symbol Contrast was weighted by a factor of 50 percent to increase the influence of Print Growth$_m$. The results for 300 RMS are shown in Table 17.

Table 17: 300 RMS (aluminum) symbol design factor results using decision heuristic. Optimum factor criterion is shown in bold.

Factor Criterion	Print Growth$_m$		Symbol Contrast		Decision Heuristic Result
	Average	Standard Deviation	Average	Standard Deviation	
Contrast Mark Spacing (diameter percentage)					
0%	79%	**1.01%**	78%	**0.478%**	**159**
25%	69%	1.10%	76%	0.697%	117
50%	54%	1.10%	78%	0.375%	153
Contrast Mark Diameter (inch)					
0.25	67%	1.26%	78%	0.51%	130
0.125	72%	**1.06%**	79%	**0.44%**	**157**
0.0625	62%	0.89%	77%	0.61%	134

To summarize the decision heuristic results indicate the symbol design criterion for contrast mark spacing is 0 percent, and contrast mark diameter is 0.125 inch. This combination of factors is expected to give the best symbol performance based on the surface prototype analysis. A 14x14 cast data matrix symbol with the capacity to contain ten alphanumeric characters with these symbol factors would have a width of 1.75 inches. A larger 24x24 cast data matrix symbol with a 50 alphanumeric character capacity have a width of 3.00 inches with these symbol factors.

Ferrous castings symbol design results were also tabulated from the experimental data using the same method as with aluminum. The results are shown in Table 18.

Table 18: Ferrous symbol design factor results using decision heuristic.

Factor Criterion	Print Growth$_m$		Symbol Contrast		Decision Heuristic Result
	Average	Standard Deviation	Average	Standard Deviation	
Contrast Mark Spacing (diameter percentage)					
0%	68%	1.62%	92%	0.122	420
25%	61%	0.59%	92%	0.094%	591
50%	56%	0.64%	91%	0.154%	383
Contrast Mark Diameter (inch)					
0.25	55%	0.94%	92%	0.143%	380
0.125	59%	0.56%	92%	0.164%	386
0.0625	71%	1.34%	91%	0.165%	134

The symbol design criterion selected by the decision heuristics was a contrast mark spacing of 25 percent, and a contrast mark diameter of 0.125 inch. For ferrous castings, a 14x14 symbol with a ten alphanumeric character capacity have a width of 2.19 inches of cast surface, while a 24x24 with a 50 alphanumeric character capacity symbol would have a width of 3.75 inches of cast surface.

The results indicate that on larger castings, the physical space required for the symbol is a feasible option, but for smaller size or small radius castings, that may not be feasible. The result indicates the symbol may not work in all applications, but will be feasible in many.

9. Conclusions

Data matrix symbols are used as a robust means of unique part identification in many industries. Research of cast data matrix symbols has been limited and expected symbol performance unknown. To develop knowledge of cast data matrix symbol performance, the investigation initially focused on feasibility of casting data matrix symbol. Results of a feasibility experiment led to further investigation of cast symbol design expected performance.

Bump marks were evaluated initially due to the inherent ease of production and use in previous cast data matrix applications. The results indicate Bump mark geometry is problematic, due to the inherent nature of shadow formation as a means to create contrast marks. Using design inspiration from Dot Peen data matrix symbols, an alternative cast data matrix design was pursued and analyzed. The results of this modified Dimple mark geometry proved to be superior to the Bump contrast symbol geometry in side by side analysis. A deeper analysis at the module level was also pursued to determine the effect on Print Growth and Symbol Contrast for an array of mark diameters, spacing and surface roughness values. Also, an optimal light angle was selected based on the ANOVA analysis and Print Growth$_m$ and Symbol Contrast averages.

An applicable design was presented with the use of a heuristic to select ideal symbol factors, which indicated the physical size for aluminum cast data matrix symbols with ten and 50 character capacities were determined to be 1.75 and 3.00 inches, respectively. Using the same methodology for ferrous cast data matrix symbols with ten and 50

character capacities, the physical symbol size was determined to be 2.19 and 3.75 inches, respectively.

During the course of this research ISO 16022 utilizes various measures to determine cast data matrix symbol quality. Cast data matrix symbols are an extension of a class of data matrix markings referred to as Direct Part Markings (DPM). ISO 16022 was developed for use with and grading of printed data matrix symbols, a two dimensional symbol that utilizes graphical representations of contrast marks. DPM, however, utilizes three dimensions to create shadows to represent contrast marks. The limitations due to the difference in scope of the standard lead to issues that, when resolved, would reduce the disconnect between symbol grades and symbol quality. The Print Growth measurement needs to be modified to incorporate the measure of centroid location of shadows relative to the identified module placement within the symbol. This approach would provide a clearer illustration of the functionality of various geometric features used to create shadows for contrast marking.

In addition, Symbol Contrast is a ISO 16022 grading criterion created to analyze data matrix symbols. The calculation of this criterion involves identifying the two pixels in the inspection space that possess the largest and smallest intensity values. This measure is subject to mischaracterization due to process variation interference caused by cast surface roughness. A useful modification to the criterion calculation should include identifying the value of average value of the highest and lowest pixel intensity

distribution quadrant, rather than the highest and lowest individual value, to avoid affects due to surface roughness.

The knowledge presented by the cast data matrix research provides a basis for practical implementation of cast data matrix symbols. Through the development of cast data matrix knowledge, opportunities to expand beyond the scope of this project was presented that should be considered as potential future work initiatives. The concepts presented in the research are related to the study of forensic investigation where lighting and the aspects of light and shadows are critical to understanding information contained within a three dimensional physical environment or crime scene. In much the same way, the three dimensional features of cast data matrix symbols interact with light to transmit identification information to a reader. A review of forensics research may reveal opportunities to improve decode and reading algorithms for the use with three dimensional symbols.

In addition, future work also includes developing a robust, high volume process for creating data matrix symbol sand cores that incorporates Dimple mark geometry. A potential approach would be to utilize the capability of an exterior, third party vendor that would specialize in the manufacture of sand cores with symbols that are then purchased by foundries for the use is sand molds, die or permanent molds, or elsewhere. Finally, utilizing methods to improve surface finish would also impact symbol performance and should be an area of focus in future experimentation. Improved surface finish would

likely lead to the ability to utilize smaller cast data matrix symbols that require less cast surface space, making the process more applicable to a wider range of part geometries.

Appendix

Surface Roughness Grading Inspection Results

Inspector	'Smooth'	120	80	40
Inspector One	20	120	420	720
Inspector Two	20	200	300	720
Inspector Three	20	200	300	560
Inspector Four	20	200	300	420
Inspector Five	20	200	300	560
Inspector Six	20	300	420	560
Mode	**20**	**200**	**300**	**560**

Bibliography

1. Altimus, J.C., V.D Johnson, M.A. Luegge, and S.N. Ramrattan. "Remote Identification of Metal Castings." *Transactions of the American Foundrymen's Society and the Proceedings of the One Hundred Second Annual Meeting* 106 (1998): 605-08.
2. Perma-Code, http://www.perma-code.com/sand_cast.html, 2009
3. Sand Casting Report – Methodology, SRC-RPT-03-002, RVSI, Don L. Roxby, 2003
4. Luther, Norris. "Considerations for a More Efficient Cleaning Operation." *Modern Casting* Jan. 2001: 29-31.
5. Askin, Ronald G., and Jeffrey B. Goldberg. *Design and Analysis of Lean Production Systems*. New York: Wiley, 2001.
6. ISO/IEC 16022 Information Technology-International Symbology Specification-Data Matrix, 1st ed., International Organization for Standardization, Geneva, Switzerland.
7. ISO/IEC 15415 Information Technology- Automatic identification and data capture techniques – Bar code print quality test specifications – Two dimensional symbols, International Organization for Standardization, Geneva, Switzerland.
8. Jangsombatsiri and Porter, Laser Direct-Part Marking of Data Matrix Symbols on Carbon Steel Substrates, June 2007.
9. Framework Software 2.7.2, Help Index Search: Print Growth Grade, 2009
10. Application of Data Matrix Identification Symbols to Aerospace Parts Using Direct Part Marking Methods/Techniques, NASA Technical Handbook, NASA-HDBK-6003B, 2006
11. Samuelson, Cory, Thomas Poole, and Jenna Geason. *3D Barcode Reading and Surface Quality*. Class Project Report. Iowa State University, 2006.
12. Juran, J. M., and Frank M. Gryna, eds. *Juran's quality control handbook*. 4th ed. New York: McGraw-Hill, 1988.
13. Columbia Marking Tools, http://www.columbiamt.com/CMT-Square-Dot-Marking/2D_Code_Size.html, 2009
14. Framework Software 2.7.2, Help Index Search: Blob Tools, 2009